



מכון ויצמן למדע
WEIZMANN INSTITUTE OF SCIENCE

Thesis for the degree
Master of Science

עבודת גמר (תזה) לתואר
מוסמך למדעים

Submitted to the Scientific Council of the
Weizmann Institute of Science
Rehovot, Israel

מוגשת למועצה המדעית של
מכון ויצמן למדע
רחובות, ישראל

By
Dan Shaked Renous

מאת
דן שקד רנו

Resistive-Plate WELL (RPWELL) gas-avalanche radiation detectors:
Methods, characterization & properties

גלאי קרינה מבוססי הכפלה בגז, "באר עם משטח בעל התנגדות":
שיטות, אפיון ותכונות

Advisor:
Dr. Shikma Bressler

מנחה:
ד"ר שקמה ברסלר

Co-advisor:
Prof. Amos Breskin

מנחה שותף:
פרופ' עמוס ברסקין

December 2017

כסלו תשס"ז

Abstract

Micro Pattern Gas Detectors (MPGD) are suitable for numerous applications in particle, astroparticle, nuclear and applied physics. The Resistive Plate WELL (RPWELL) was designed to overcome one of the first challenges of the MPGD – the discharge problem. Since it was presented in 2013 by the Weizmann radiation detection group, the RPWELL detector has been investigated at the laboratory and at CERN test-beam facilities demonstrating broad dynamic range, efficient and stable discharge-free operation and stable high gain over time - in neon and argon based gas mixtures under X-ray source and under muon and high rate pion beams. In this thesis, two studies which continue the characterization of the RPWELL in Ne/CH₄ (95:5) are presented as part of the ongoing research and development towards future applications. The first is a systematic comparison of RPWELL materials and production techniques aiming to overcome the weak points of the current FR4 and the Semitron ESD225® materials, which were used in the previous RPWELL studies. Configurations comprise Low Resistive Silicate (LRS) glass resistive plate, single sided THGEM electrode made of alumina and an epoxy-made electrode with a novel design of a step-WELL will be compared to the regular RPWELL realization. In the course of this study a systematic methodology for RPWELL characterization was developed, revisited and improved. In addition, a first long-term gain stabilization process (GSP) characterization was performed across days of spectra acquisition. This experiment showed intriguing trends of GSPs due to changes in the operation voltages and due to changes in the X-ray source rate in the different configurations. The second study presents a first UV photon detection characterization of RPWELL-based single and dual stage detectors. Exciting results are presented as both configurations yield a clear single-electron avalanche size distribution, which shows the Polya distribution peak paving the way to an effective single UV photon detector.

Acknowledgments

I would like to express my deep gratitude and appreciation to my colleagues, without whom this thesis would not be completed. Their assistance, support and encouragement were invaluable. In particular, I would like to extend my special thanks:

To my supervisors, Dr. Shikma Bressler and Prof. Amos Breskin who gave me the opportunity to find my own place and way in the field of experimental research, giving good advice and sharing their expertise in the field of radiation detection.

To Dr. Lior Arazi for the patience and the enthusiasm which accompanied his guidance whenever a difficulty came up.

To my friends and colleagues in the Weizmann Radiation Detection group Dr. Artur Coimbra, Eran Erdal, Itamar Israelashvili, Luca Moleri, Michael Pitt, Dr. Arindam Roy and Dr. Sergei Shchemelinin for the productive discussions and assistance.

To Yehuda Asher, Amir Bar-On, Yafa Gil, Moshe Klin, Dr. Michael Rappaport and Yigal Shahar for their warm personality and technical help.

Finally, I would like to thank my wife Lior and daughter Sophia, for their love, support and encouragement.

Table of Contents

Abstract	2
List of abbreviations	6
1 Introduction	7
1.1 Basic Processes in Gas-Avalanche Radiation Detectors – A concise review	9
1.1.1 Interaction of massive charge particles with matter	9
1.1.2 Photon-gaseous interactions.....	10
1.1.3 Primary electrons formation	11
1.1.4 Electron amplification in THGEM-like detectors.....	11
1.2 Gain Variations and stabilization.....	13
2 Systematic comparison of RPWELL materials and production techniques	14
2.1 Introduction.....	14
2.2 The step-WELL geometry	15
2.3 Production Techniques and Materials.....	17
2.3.1 Electrode types.....	17
2.3.2 Resistive materials	19
2.4 Apparatus & Methodology	19
2.4.1 Experimental setup.....	19
2.4.2 Methodology	20
Gain-vs.-voltage measurements	21
2.5 Results.....	22
2.5.1 Signal Shape.....	22
2.5.2 Spectra.....	23
2.5.3 Gain Measurements	24
2.5.4 Gain stabilization	27
2.6 Discussion on section 2 results	33
2.6.1 Signal shape	33

2.6.2	Energy resolution.....	33
2.6.3	Gain measurements.....	33
2.6.4	Gain stabilization.....	34
2.7	Conclusions.....	37
3	First characterization of UV-photon detection in RPWELL-based detectors.....	39
3.1	Introduction.....	39
3.2	Apparatus & Methodology.....	40
3.2.1	Experimental setup.....	40
3.2.2	Methodology.....	41
3.3	Results.....	43
3.4	Discussion on section 3 results.....	45
3.5	Conclusions.....	46
4	General summary.....	46
5	References.....	47

List of abbreviation

ADC – Analog to Digital Converter
CsI – Cesium Iodide
DHCAL – Digital Hadron Calorimeter
ESD – Electrostatic Dissipative
FWHM – Full Width at Half Maximum
GEM – Gaseous Electron Multiplier
GSP – Gain Stabilization Process
GPM – Gas Photomultiplier
HV – High Voltage
LPF – Low Pass Filter
LRS - Low-Resistivity Silicate
MCA – Multi-Channel Analyzer
Micromegas – Micro Mesh Gaseous Structure
 μ -RWELL – Micro Resistive WELL
MIP – Minimum Ionizing Particle
MPGD – Micro-Pattern Gaseous Detector
MWPC – Multi-Wire Proportional Chamber
PCB – Printed Circuit Board
PDE – Photon Detection Efficiency
QE – Quantum Efficiency
RICH – Ring Imaging Cherenkov
RP – Resistive Plate
RPC – Resistive Plate Chamber
RPWELL – Resistive Plate WELL
RWELL – Resistive WELL
THGEM – Thick Gaseous Electron Multiplier
THWELL – Thick WELL

1 Introduction

The Thick Gas Electron Multiplier (THGEM) [1] is a robust radiation detector element suitable for a large number of applications such as Ring Imaging Cherenkov (RICH) devices [2], cryogenic detectors for neutrino physics TPC [3, 4], Gaseous Photomultipliers (GPM) for dark matter searches [5], medical imaging [6], fast-neutron and γ imaging in cargo inspection systems [7, 8], thin sampling elements for DHCAL [9] and more. Its main purpose is to amplify and detect radiation-induced ionization electrons. The electron multiplication process is driven by the development of avalanche multiplication within sub-millimeter diameter holes drilled typically in a 0.8 or 0.4 mm thick FR4 (or other) insulator plate, Cu-cladded on both sides.

Highly ionizing background environment in some applications can result in the formation of large avalanches, thus causing electric discharges. The latter can damage the readout electronics and the detector itself and often introduce significant dead-time to the detector operation. The discharge problem is a known challenge in gaseous radiation detectors, known long before the introduction of the THGEM. Therefore, following past experience with other gaseous detectors (for example the Resistive Plate Chamber (RPC) [10] and the Thin Gap Chambers [11], the micro-pattern gas detector (MPGD) community [12] puts an effort in conceiving ways for mitigating or eliminating discharges in new types of detectors, by applying resistive electrodes. Examples are: Resistive Micromegas [13], Resistive WELL (RWELL) [14], Micro Resistive WELL (μ -RWELL) [15], the Resistive-Plate WELL (RPWELL) [16] [17] etc.

The RPWELL, the subject of this work, is shown in Figure 1. It is a THGEM-like detector comprising a single-sided THGEM electrode coupled to a readout anode via a resistive plate. The radiation-induced electrons are collected into the THGEM holes. These electrons are produced either by gas ionization or from radiation converting materials deposited on the THGEM-top electrode surface, such as cesium iodide (CsI) photocathode. The high voltage (HV) applied across the THGEM electrode gives rise to an intense electric field within the holes, which accelerates the electrons such that they accumulate enough energy to undergo avalanche multiplication. The motion of the electrons toward the anode and the ions away from it induces a detectable signal [18, 19] which can be recorded through the readout electronics. Occasionally, highly ionizing background particles enter the detector, yielding an avalanche of a size greater than 10^6 - 10^7 electrons¹, reaching the theoretical onset of discharges propagation (the Raether limit [20]). The role of the resistive-plate, placed between the THGEM and the readout anode, is to prevent or quench these eventual discharges.

¹ Large avalanches can be induced also by minimum ionizing particles. The Landau distribution describing their energy deposition spectrum has a long tail.

This solution was inspired by the RPC, where a high resistivity plate ($\rho = \sim 10^{12} \Omega cm$) limits geometrically the discharges to a relatively small area of 10 mm^2 [21]. This means that when a discharge is created it causes a local voltage drop. The addition of the resistive plate on the anode, creates an effective RC circuit with relaxation time $\tau = \rho \epsilon$ (ϵ is the material permittivity). This is also the time which takes the power supply to recharge the electrodes and regain voltage. This typical scale of resistivity values yields τ at the order of milliseconds. This is significantly longer than the typical time scale needed to maintain a discharge which is at the order of nanoseconds. Hence, the electrodes act de facto as insulators and the discharge is extinguished [22].

The RPWELL was introduced in 2013 by the Weizmann Radiation Detection group [16, 23] with preliminary results that suggest a potential for a simple robust single-stage detector with stable operation over a broad dynamic range. Further systematic investigations have been done with this single detector element by the group since, at the laboratory and at the CERN-RD51² test beam. They demonstrated a high detection efficiency of minimum ionizing particles (MIPs), over a broad particle-flux range - in a discharge-free operation mode at high gain [24 - 26].

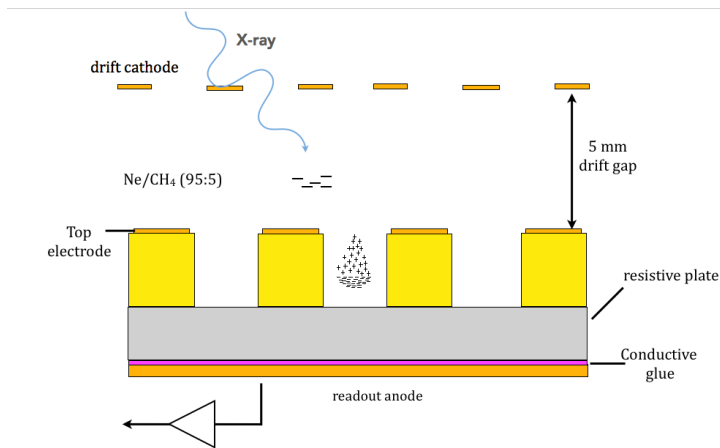


Figure 1: Standard RPWELL configuration: 0.8 mm thick, 0.5 mm hole diameter, 0.1 mm rim and 1 mm pitch Cu-clad FR4 single-sided THGEM; 0.4 mm thick Semitron ESD225 resistive plate; -1050 V and -900 V is applied on the drift electrode and the THGEM top electrode, respectively; a 5.9 keV X-ray source would be converted to ~ 164 primary electrons which would drift into the holes and would result in an avalanche of $\sim 10^6$ electrons.

In this work, we present two additional studies towards the potential application of the RPWELL detector concept. The first is a systematic comparison of different RPWELL detector realizations, using various THGEM electrode materials, production methods and different resistive-plate materials. As part of this study a new THGEM-like electrode with a step-WELL hole geometry is introduced, proposed to enhance the operation stability. An important part of the thesis work has been devoted to the development of a solid methodology for efficient comparative detector-characterization studies. It enabled evaluation

² The research and development number 51 (RD51) collaboration at CERN is devoted to the development of MPGD

of the time scales associated with the RPWELL stabilization in the transition between various operation conditions and paved the way towards deeper understanding of the physics process involved in the RPWELL stabilization.

A second study is that of a novel UV-photon detector concept comprising a single- and a dual-stage RPWELL coated with a UV-sensitive CsI photocathode.

1.1 Basic Processes in Gas-Avalanche Radiation Detectors – A concise review

Gas-avalanche detectors count among the leading tools for charged-particles, X-ray and UV-photon as well as neutron imaging. The detection is achieved by avalanche multiplication of radiation-induced electrons. These are deposited in the detector volume by energy-loss processes of charged or neutral particles or emitted from a photocathode by an interacting photon.

1.1.1 Interaction of massive charge particles with matter

The energy loss of a charged particle due to electromagnetic interactions with the detector medium can be expressed by the Bethe-Bloch formula

$$\frac{dE}{dX} = -K \frac{Z}{A} \frac{\rho}{\beta^2} \left[\ln \frac{2mc^2 \beta^2 E_M}{I^2 (1 - \beta^2)} - 2\beta^2 \right]; \quad K = \frac{2\pi N z^2 e^4}{mc^2} \quad (1)$$

Where m and e are the electron mass and charge; Z, A and ρ are the medium atomic number, atomic mass and density, respectively; β and z are the detected particle velocity in units of c and charge; I is the effective ionization potential of the medium; E_M is the maximal energy transfer allowed in each interaction and N is the Avogadro number. Using this equation, it can be shown that at the energy region between $\sim 100\text{MeV}$ to $\sim 10\text{GeV}$ the energy loss reaches a minimum and all the charged particles are MIPs [27].

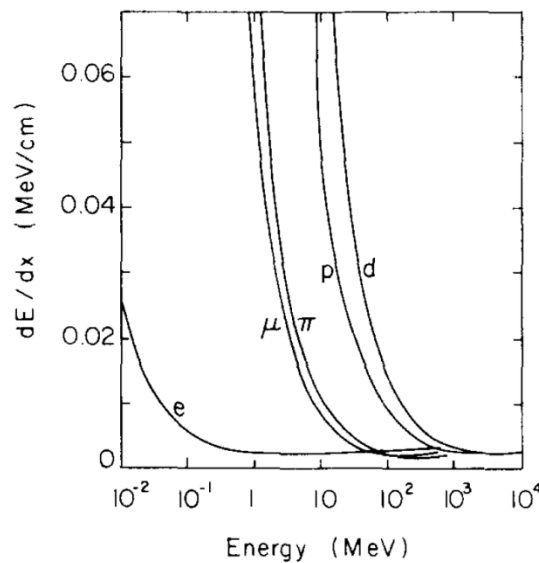


Figure 2: Energy loss per unit length in air, as computed from equation (1), for different particles as a function of their energy. At energies above 1 GeV/c or so, all particles lose about the same amount of energy (minimum ionization plateau) [27].

1.1.2 Photon-gaseous interactions

Photon beams interacting with a medium undergo attenuation. The resulting flux I is expressed by

$$I = I_0 e^{-\frac{X}{\lambda}} \quad (2)$$

where I_0 is the initial flux; X is the medium thickness; the mean path is $\lambda = \frac{1}{\mu\rho}$; μ and ρ are the mass attenuation coefficient and density, respectively. In the case of low energy photons - up to several keV - the dominant process is photoelectric conversion [27]. For energies above a few keV the main absorption is by the K-shell which yields the emission of a photoelectron of energy $E_{pe} = E\gamma - E_k$, where $E\gamma$ is the photon energy and E_k is the binding energy of the K-shell, followed by the gas molecule/atom de-excitation.

The fraction of de-excitations producing the emission of a photon is called fluorescence yield. As can be seen in Figure 3 the fluorescence yield of the K-shell increases with the atomic number.

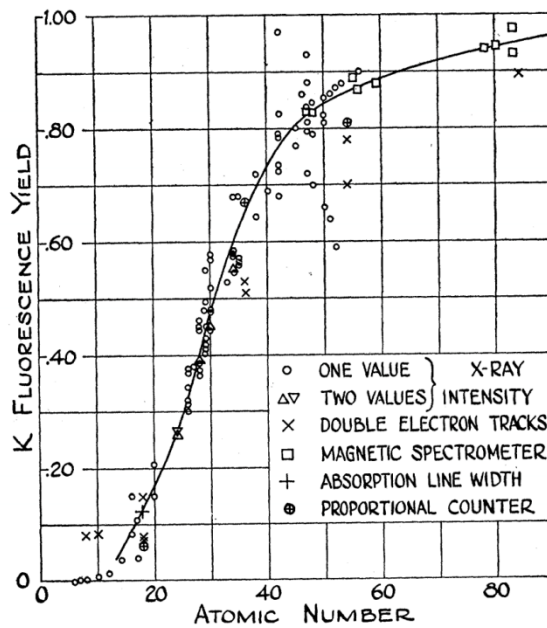


Figure 3: K Fluorescence yield [28]

While in neon, fluorescence yield is negligible, photon emission in argon follows 15% of the photoelectric absorptions. The secondary photon, emitted at energy just below the K-edge, has a very long mean free path for absorption and can therefore escape from the volume of detection. This produces the characteristic escape peak of argon, at an energy $E\gamma - E_k$. The rest of the events produce two

electrons, one heavily ionizing photoelectron of energy $E_\gamma - E_K$ and an Auger electron of energy slightly smaller than E_K [27].

A UV photon, of a few eV energy, interacts with either a low-ionization potential “photosensitive” gas or with a solid photocathode; the latter is usually deposited on the detector’s electrode [29]. In the case studied here, a UV-sensitive CsI photocathode can be deposited on the RPWELL top electrode. In this operation mode, there is only one (eV) primary electron emitted per interacting photon.

1.1.3 Primary electrons formation

The motion of the primary electrons, deposited either by a MIP or by photoelectric interaction, is quickly randomized by multiple scattering, during which they can produce secondary electron-ion pairs. The total number of pairs can be expressed by

$$n_T = \frac{\Delta E}{W_i} \quad (3)$$

Where n_T is the number of the total electron-ion pairs; ΔE is the energy deposited by the incoming particle in the detector, and W_i is the effective average energy to produce one electron-ion pair. The values for W_i neon, argon and methane are 36, 26 and 28 respectively, and in the case of gas mixture it is the weighted average of the relevant W_i values [27].

1.1.4 Electron amplification in THGEM-like detectors

Typically, the energy conversion process in THGEM-like detectors (Figure 1) takes place in the drift gap of the detector. There, the primary electrons drift along the electric field into the THGEM holes. In case of MIPs and X-ray photons, a drift field of approximately 0.5 kV/cm is applied between the drift cathode and the RPWELL top electrode; the drifting electrons are focused into the holes by the dipole field - resulting of the application of a potential across the holes, where they undergo avalanche multiplication. For the UV detection the drift field is not necessary (one avoids collecting background particles) and the sole dipole field permits the efficient collection of the photoelectrons into the holes, for consequent multiplication.

The electron multiplication is done by an avalanche effect. Considering an electron inside a strong electric field, as inside the RPWELL holes, its mean free path for ionization is defined as the average distance it travels before it is involved in an ionizing collision. Thus, an electron in a uniform electric field will produce, on the average, one electron-ion pair after a mean free path; the two electrons will generate, after another mean free path, two additional pairs and so on. Hence, the inverse of this mean free path represents the average number of electron-ion pairs produced per unit length; this so-called the

first Townsend coefficient, α , [27] allows getting an expression for the increase in the number of electrons n after a path dx as $dn = n\alpha dx$; the detector's gain G is expressed as:

$$G = \frac{n}{n_0} = \exp \left[\int_{x_1}^{x_2} \alpha(x) dx \right] \quad (4)$$

or for the simple case of a uniform field, $G = e^{\alpha x}$.

The statistics of single-electron avalanche states that the probability $P(n, x)$ of a single primary electron to produce an avalanche with n electrons while propagating from the origin to a point x follows an exponential law in moderate electric field

$$P(n, x) \simeq \frac{1}{\bar{n}(x)} e^{-\frac{n}{\bar{n}(x)}} \quad (5)$$

In a high electric field, it is assumed that the avalanche electrons can be divided into two classes: “fast electrons” – with energies much larger than the ionization energy of the gas – and “slow electrons” with energy below the ionization threshold. The probability of a single primary electron to produce an avalanche with n electrons while propagating from the origin to a point x follows a Polya distribution [30]

$$P(n, x) = \left[\frac{(1 + \theta)n}{\bar{n}(x)} \right]^\theta e^{-\left[\frac{(1+\theta)n}{\bar{n}(x)} \right]}; \quad \theta = \frac{\lambda(x)}{\mu(x)} \quad (6)$$

where $\lambda(x)$ is the probability per unit length that a fast electron would participate in an ionizing collision assuming that one fast electron and one slow electron would emerge from such a collision; and $\mu(x)$ is the probability per unit path length that a slow electron would accumulate enough energy to become a fast electron. In a given detector configuration larger θ gives larger single-electron detection efficiency.

For X-ray interactions, resulting in many ($>10^2$) primary electrons, each single electron-avalanche size, n_i is independent and have the same avalanche distribution, $P(n)$, with mean value \bar{n} and variance σ^2 . The central-limit theorem of statistics states that if $k \rightarrow \infty$, then the probability function, $F(N)$, of the total avalanche size, N , which applies $N = \sum_{i=1}^k n_i$, is a Gaussian [31]

$$F(N) = \frac{1}{S\sqrt{2\pi}} e^{-\frac{(N-\bar{N})^2}{2S^2}}; \quad S^2 = k\sigma^2; \quad \bar{N} = k\bar{n} \quad (7)$$

Secondary processes, like photon emission, can induce secondary avalanches which can result in a spark breakdown. A phenomenological limit for multiplication before breakdown is given by the Raether condition as $\sim 10^8$ [20], however statistical fluctuations lower the average operational multiplication to $\sim 10^6$.

As mentioned before, inside the RPWELL holes the electrons move under a very intense electric field ($\sim 20\text{kV/cm}$ for a 0.4 mm deep hole applied with 1kV), which let them accumulate enough energy between two collisions to induce excitation and ionization. While noble gases can be excited only through

photon absorption or emission, molecules can have many modes of excitation, such as radiation-less transitions of a rotational and vibrational nature, depending on their complexity. This quenching property turns out to be beneficial. By adding such gas vapors to noble gases, a significant fraction of energy from secondary effects dissipates to radiation-less modes, which allows the detector to reach high gain and stable operation [27]. In the presented studies below, a Ne based mixture with 5% methane (CH₄) as a quencher was used.

Since the ions' drift velocity is lower by three orders of magnitude than the electrons' one, the avalanche has a drop-like structure, where the electrons are concentrated in the avalanche "head" and spread due to electrostatic repulsion and diffusion. The implications of the lateral dynamics of the charge inside the RPWELL holes will be discussed later on.

The avalanche charge movement in the vicinity of the anode induces an electric current in the anode which is recorded by the readout electronics as a signal. This signal can be calculated using Ramo's theorem. The current induced on a grounded electrode by a point charge q moving along a trajectory $x(t)$ is

$$I_n^{ind}(t) = -\frac{q}{V_w} E_n[x(t)]v(t) \quad (8)$$

where $E_n(x)$ is the *weighting field*, the electric field in the case where the charge q is removed, electrode n is set to voltage V_w , and all other electrodes are grounded [31]. This calculation principle can be applied to different detector geometries. This type of calculations is not within this project's scope and can be found for example in Blum, Riegler and Rolandi [31].

1.2 Gain Variations and stabilization

In THGEM-like detectors, two main factors affect the detector gain after its initialization: the electric field configuration and the gas density (temperature and pressure).

Variations in the electric field are mainly caused by the presence of space-charge in the multiplication region. The THGEM-electrode insulator undergoes two competing processes – charge accumulation (charging up) and charge evacuation. The charging up is caused by lateral diffusion of the avalanche charge, such that the electrons occupy the lower part of the walls and the ions the upper part [32]. This charge distribution creates an electric field in the opposite direction compared to the original field which reduces the gain where ions and electrons are accumulated on the holes' walls. On the other hand, the charge evacuation process is more complex and a few mechanisms can participate in it, e.g. gas recombination, conductance by humidity and by the electric field applied between the electrodes. The latest charge clearance model for THGEM-like detectors was suggested at [33]. They proposed that "A movement of charges takes place in the PCB (printed-circuit board) fiberglass plates when there are electrodes in contact with the plate and connected to a power supply; this effect, not to be confused with

the dielectric polarization, has been observed in glass and it is due to a displacement of charges in the material related to the mobility of charges in the insulator bulk; the displacement is slow: it takes hours or days before an asymptotic configuration is reached". Both effects in the RPWELL and in THGEM in general are under study by our group and other members of the RD51 collaboration.

Variations in the gain associated with variations in the gas density are explained by the fact that the Townsend coefficient depends on the gas temperature and pressure. In [34] the relation between the gain and the gas temperature and pressure is derived in the context of GEM-based detectors and assumes $\alpha \sim n \sim T/p$, that is $G = Ae^{B\frac{T}{p}}$, thus allowing to derive a normalized gain function of temperature and pressure variations

$$G_{norm} = \frac{G}{Ae^{B\frac{T}{p}}} \quad (9)$$

Somewhat contradictory, in [35] it was derived in the context of Micromegas detectors and claimed that $\alpha \sim n \sim P/T$ and so

$$G = \exp\left[\frac{APg}{T} \cdot \exp\left(-\frac{Bpg}{TV}\right)\right] \quad (10)$$

where g is the avalanche-multiplication gap of the detector and V is the voltage between the gap planes. Both derivations are independent of the detector geometry, i.e. if it is a GEM, Micromegas, a wire chamber or a THGEM based detector.

In the work presented here temperature variations did not affect the conclusions obtained, hence no corrections were applied.

2 Systematic comparison of RPWELL materials and production techniques

2.1 Introduction

In the last couple of years, the RPWELL [16] was thoroughly investigated at the laboratory and at CERN test-beam facilities [24-26]. It demonstrated stable discharge-free operation and stable gain over time - in Neon and Argon based gas mixtures under muon and high rate pion beams. Furthermore, the detector reached high detection efficiency, close to 100%, over a broad range of ionizing particles. These results proved the feasibility of the RPWELL concept and served as a motivation toward further improvements of its design and manufacture techniques.

The most commonly used THGEM electrode is made of a mechanically drilled copper clad FR4 plate (standard PCB production technique). This production technique is both time consuming and expensive; the drilling itself is time consuming (~50 hours for 1 m² electrode) and it requires expensive

post-treatment to remove residual spikes within the multiplication holes. The best resistive plate material found so far is Semitron ESD225³; it has a bulk resistivity in the range of 10^9 - 10^{11} Ωcm suitable for most applications, but suffers a large thermal expansion and is hygroscopic. Its electrical properties and radiation hardness (both are needed for many application in particle physics) were not tested.

These shortcomings of the technology and materials used, as well as the environment criteria imposed by different potential applications of the RPWELL, such as sampling elements for Digital Hadron Calorimetry (DHCAL) in high energy physics experiments [36], motivate the search for new production techniques and materials. In this work, we present a systematic comparative study of RPWELL configurations of new materials and new WELL electrode geometry.

Based on previous studies [24-26], the baseline configuration was defined to be the 0.8 mm thick FR4-made THGEM with 0.4 mm Semitron resistive plate (RP). To assess the effect of the RP, a bare-WELL configuration – 0.4 mm thick FR4-made WELL (THWELL) with no RP – provided with a reference measurement. The tested configurations are summarized in Table 1.

Geometry	Electrode Material	Resistive Material	Bulk Resistivity
<i>0.8 mm*</i>	<i>FR4 - Cu</i>	<i>0.4 mm Semitron</i>	<i>$10^9 \Omega\text{cm}$</i>
<i>0.4 mm*</i>	<i>FR4 - Cu</i>	-	-
<i>0.4 mm</i>	<i>FR4 - Cu</i>	<i>0.4 mm Semitron</i>	<i>$10^9 \Omega\text{cm}$</i>
<i>0.4 mm</i>	<i>FR4 - Cu</i>	<i>0.7 mm LRS glass</i>	<i>$10^{10} \Omega\text{cm}$</i>
<i>0.8 mm</i>	<i>FR4 - Cu</i>	<i>0.7 mm LRS glass</i>	<i>$10^{10} \Omega\text{cm}$</i>
<i>0.4 mm</i>	<i>Alumina – Cu</i>	<i>0.4 mm Semitron</i>	<i>$10^9 \Omega\text{cm}$</i>
<i>0.4 mm step</i>	<i>Epoxy-Ni</i>	<i>0.4 mm Semitron</i>	<i>$10^9 \Omega\text{cm}$</i>

*Reference measurements

Table 1: List of the different configurations & materials investigated

2.2 The step-WELL geometry

The step-RPWELL configuration (Figure 4) is based on a WELL electrode in which the holes are made of two different diameters. In the epoxy electrode used throughout this study, the top half of the hole has a 0.5 mm diameter, while the bottom half is of 0.7 mm diameter. It was first suggested in order to increase the path length between the top electrode and the anode and thus reduce potential leak currents and associated instabilities.

Another potential advantage of the step-RPWELL configuration is the possibility to reduce the

³ <http://www.quadrantplastics.com>

charging up of the WELL holes - a major source of gain instability in the RPWELL. The charging up of the WELL holes is attributed to the diffusive dynamics of the electrons and (at a lower level) the ions which allows them to reach the holes insulating walls. As mentioned in section 1.2, this effect modifies the field configuration inside the holes and thus reducing the gain of the multiplier. In such geometry, the walls at the last steps of the avalanche are distant from the electrons.

The field in a step-WELL configuration is very similar to the field in a standard RPWELL configuration as confirmed using COMSOL Multiphysics®⁴ simulation toolkit (Figure 5a). The only exception is the region close to the edge of the step in which the field is higher (Figure 5b).



Figure 4: Step-RPWELL configuration

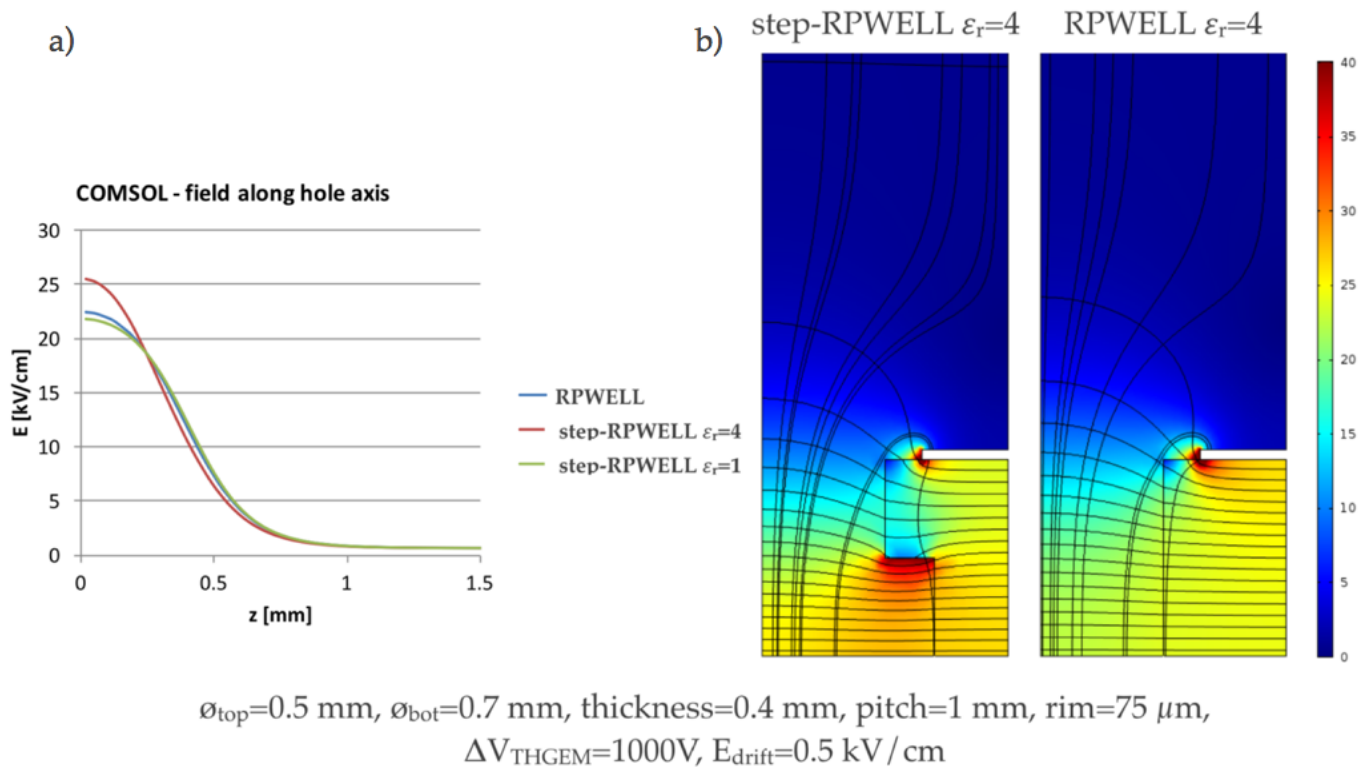


Figure 5: COMSOL electric field simulations of a step-RPWELL and RPWELL configurations. The color scale on the right represents the electric field magnitude in units of kV/cm.

⁴ <http://www.comsol.com>

2.3 Production Techniques and Materials

2.3.1 Electrode types

2.3.1.1 0.8 & 0.4 mm thick FR4

The “standard” Cu-clad FR4 THGEM electrodes are manufactured by standard PCB techniques. The holes are mechanically drilled with a computer numerical control (CNC) machine. 100 μm rims are chemically etched around the holes. The drilling tends to leave sharp edges inside the holes and in the Cu; these are weak points – prone to discharges. This demands electrode’s post-treatment. Hence the overall production process is time consuming, expensive and could be problematic for large-area applications. The FR4 electrical properties are depicted in Table 2. Figure 6 shows a photograph of FR4-made THGEM electrode.

Dielectric constant:	4.34 (1GHz)
Dielectric strength:	$\sim 20 \text{ V}/\mu\text{m}$
Bulk resistivity:	$10^{14} \Omega\text{cm}$ (at 25°C)

Table 2: FR4 electrical properties

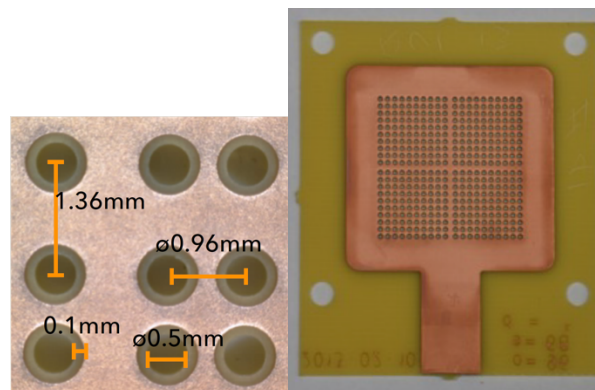


Figure 6: FR4 THGEM electrode (right) and typical dimensions (left)

2.3.1.2 0.4 mm thick alumina

The Alumina THGEM electrode (Figure 7) was Cu coated using mesh screen print, leaving 65 μm rims around the holes. The holes were produced by laser cut technology. The latter yields slightly conical holes as can be seen in Figure 8. This process requires improvement; the sample-electrodes used in this study had areas depleted of Cu, eccentric rims around holes and sharp edges in some of the holes (Figure 9).

Dielectric constant:	9.5 (1 GHz)
Dielectric strength:	$\sim 23.6 \text{ V}/\mu\text{m}$

Resistivity:	$> 10^{14} \Omega\text{cm}$ (at 25°C)
--------------	---------------------------------------

Table 3: Alumina electrical properties

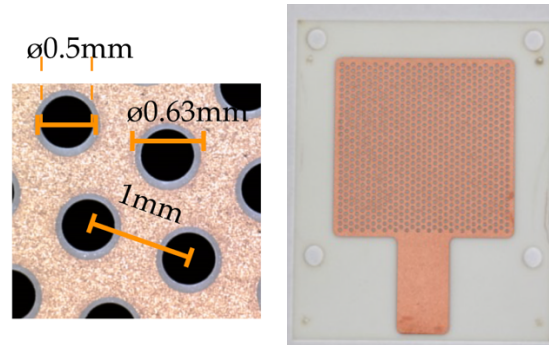


Figure 7: Alumina electrode (right) and typical dimensions (left).

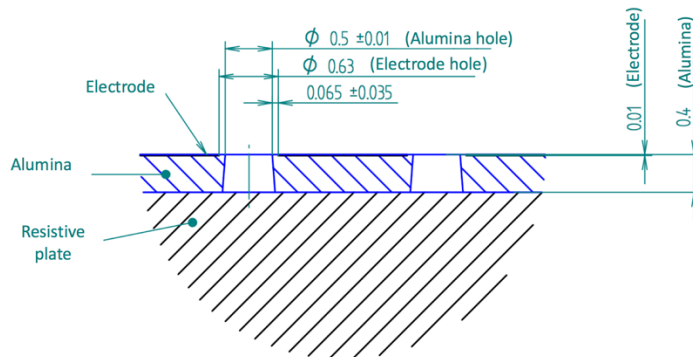


Figure 8: Schematic cross section of the alumina electrode. The dimensions are in millimeters.

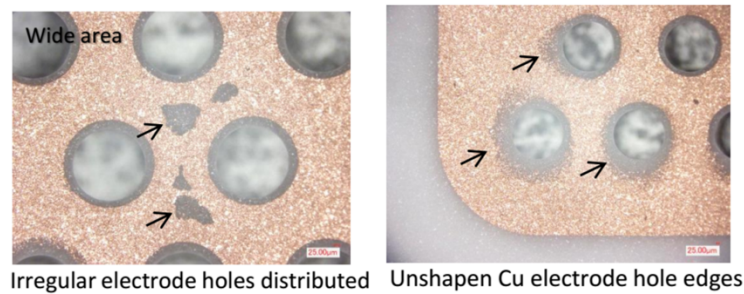


Figure 9: Alumina THGEM electrode sample with defects. Eccentric rims (right) and regions without Cu (left).

2.3.1.3 0.4 mm thick Epoxy step-WELL

The epoxy electrode (see Table 4 for electrical properties) was produced from epoxy-based SU-8 negative photoresist in a photo-lithography technology. The parts of the SU-8 polymer which are exposed to UV light become cross-linked, while the rest parts remain soluble and washed away during development. This technique allows a very precise manufacturing (Figure 10). The electrode's conductive material was nickel which attaches better than copper to epoxy⁵. The precise production of the step design

⁵ Private communications with the manufacturer: OPTNICS Japan (<http://www.optnics.co.jp/en/>)

yielded sharp edges at the holes' edges and at the step between the two diameters. The rim size was 75 μm .

Dielectric constant:	3-4 (1 GHz, 50%RH)
Dielectric strength:	110-120 V/ μm
Resistivity:	10^{16} Ωcm (at 25°C)

Table 4: Epoxy electrical properties

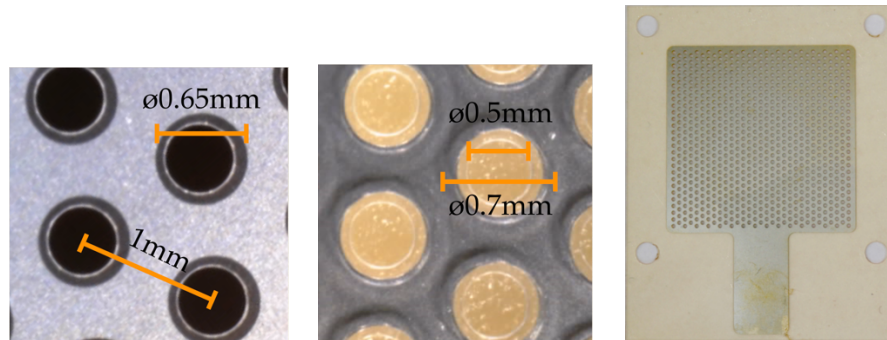


Figure 10: Epoxy 0.4 mm step-WELL electrode (right).
Dimensions of the top side (left) and of the bottom side (center).

2.3.2 Resistive materials

In addition to the study of different electrodes, we performed a comparison between two resistive materials - Semitron ESD 225⁶ with bulk resistivity 10^9 - 10^{11} Ωcm and low-resistivity silicate glass (LRS glass)⁷ with bulk resistivity $\sim 10^{10}$ Ωcm [37].

2.4 Apparatus & Methodology

2.4.1 Experimental setup

In these experiments, we used a Cu-target X-ray tube⁸ as 8 keV photon source, illuminating the detector through a 50 mm diameter thin Kapton window (shown in Figure 11). The X-ray flux was controlled by varying the current of the X-ray tube and by Cu filters, 0.5 mm and 0.2 mm thick, placed before the 1.5 mm diameter collimator. Power to the drift electrode and the RPWELL top was supplied through a low-pass filter (LPF) using CAEN⁹ HV A1651H module and SY5527 mainframe; the current and voltage monitoring was done using CAEN GECO2020 software. The signals were read from the anode through an Ortec¹⁰ 125 charge sensitive preamplifier; they were processed either by an Agilent

⁶ <http://www.quadrantplastics.com>

⁷ Obtained from Prof. Yi Wang, Tsinghua University

⁸ Oxford Instruments Apogee 93500 radiation shielded tube

⁹ <http://www.caen.it>

¹⁰ <http://www.ortec-online.com>

technologies InfiniiVision DSO-X 3034A oscilloscope, for signal shape acquisition, or by an Amptek¹¹ 8000a pocket MCA through an Ortec 572 linear amplifier for spectra acquisition.

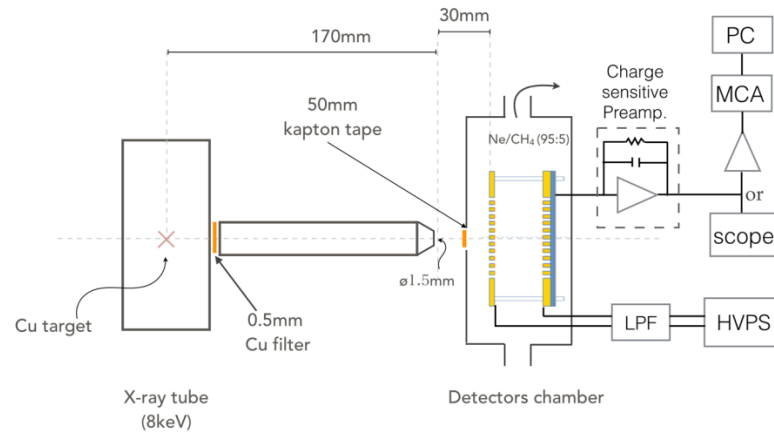


Figure 11: Experimental setup

2.4.2 Methodology

Systematic comparison between different detector configurations was performed using the same measurements protocol when testing each configuration. The development of the methodology consists an important part of the work. It aims at standardizing a characterization protocol for RPWELL-based detectors which was not available. Two methods were used; the first for detector gain vs. voltage recording and the second for the study of gain stabilization in time.

2.4.2.1 Methodology for gain measurements

Except for the 0.8 mm FR4 Semitron RPWELL set of measurements, all configurations had “clean” history, i.e. they were not exposed to charging up effects prior to the comparative sets of measurements. The protocol was established as follows:

Initial preparations

Once a detector was mounted inside the (Aluminum vessel) test chamber, it was flushed with Ne/CH₄ (95:5) at a flow rate of 100 sccm for 1 hour; the flow was then reduced to 20 sccm. After waiting for 30 minutes for a stabilization of the gas flow in the system, the X-ray tube was activated. The tube was operated at 25 kV with a current set to yield a detector counting rate of 30 Hz/mm² after the 0.5 mm thick Cu-filter. The voltages on the top electrode and the drift cathode were gradually increased, while maintaining a drift field of 0.5 kV/cm - until small signals appeared on the oscilloscope.

¹¹ <http://amptek.com>

Gain-vs.-voltage measurements

The voltages on the top electrode and the drift cathode electrodes (Figure 1) were ramped up and stabilized. The current supplied to the top electrode was monitored. In order to measure transient effects related to the exposure to radiation, prior to turning on the X-ray tube, the MCA was set to conduct multiple repetitive 60 sec long acquisitions. The measurements set ended upon the appearance of visible current spikes – larger than 2 nA. Otherwise, the gain was monitored until it reached stabilization. Once stabilized, the X-ray tube was switched off and the voltages applied to the top electrode and the drift cathode were increased by 50 V.

2.4.2.2 Methodology for long term stabilization measurements

As observed in many previous works on GEM [38-40] and THGEM [41,42] the detector gain varies in time according to charge and field variations in the holes. The process of reaching equilibrium of charge accumulation and evacuation within the holes and on the RP is defined here as gain stabilization process (GSP). The GSP of an electrode depends on many parameters and on the detectors history; for example, an electrode exposed to air (e.g. to humidity) prior to the measurements behaves differently than one irradiated after long gas circulation or under high-vs-low flux, or measured after its operation voltage was reduced. Therefore, gain stability results should always be presented with the detector history. Hence, in order to perform a systematic comparison of the detector stability a new methodology was developed. It was based primarily on keeping equal history for all detector configurations investigated. This methodology development effort has been a long ongoing process which evolved to take into account various phenomena observed along the measurements (see section 2.6).

The response of the gain to two types of extreme modifications of the operation conditions were investigated sequentially – changes of the voltage applied on the multiplication region and changes in the incoming particle flux.

Initial preparations

Trying to equalize the initial conditions of the electrodes, the tested electrode was exposed to air and flushed for ~1 minute with ionized nitrogen using an electrostatics Inc.¹² 190M anti-static gun. This flow of ions and electrons onto the THGEM electrode, neutralized the accumulated charge on it. Once cleaned, the detector was assembled inside the test chamber where it was flushed with Ne/CH₄ (95:5) at a flow-rate of 20 sccm for 4 days.

¹² <http://www.electrostatics.com>

Long term stabilization measurements

Step 1: Initial stabilization at a low gain and low irradiation rate: after the initial preparation, the detector electrodes were biased. The chosen voltage was selected to yield a gain of ~ 1000 : for a 0.4 mm (0.8 mm) the top electrode was set to 700 V (800 V) – while maintaining a 0.5 kV/cm drift field between the cathode and the top electrode. The data acquisition started once the voltage reached its set values: using the MCA, consecutive spectra were measured for the entire duration of the measurement (days). Each spectrum was acquired for 60 sec and two consecutive spectra were separated by 10 sec. Immediately after the acquisition started, the X-ray tube was switched on; it was operated at 25 kV with a current yielding a detector counting- rate of 30 Hz/mm² (after the 0.5 mm thick Cu-filter attenuation). The measurements lasted for at least one day after stabilization was obtained.

Step 2: Stabilization in the transition between low- and high-gains at low irradiation rate: the operation voltages of the detector were raised to reach a gain higher by a factor of 5 or 10. When the gain was stable for a few hours, the voltages were reduced to their initial values. No additional modifications were done before the gain stabilized.

Step 3: Stabilization in the transition between low- and high-irradiation rates at low gain: a few cycles of increasing and lowering the rate from ~ 30 Hz/mm² (with the 0.5 mm thick Cu-filter) – to ~ 1.3 kHz/mm² (with a 0.2 mm thick Cu-filter) – and back to ~ 30 Hz/mm² were performed. At each rate, we waited for gain stabilization. During the changes of rate, the X-ray source was stopped for 30 seconds.

2.5 Results

2.5.1 Signal Shape

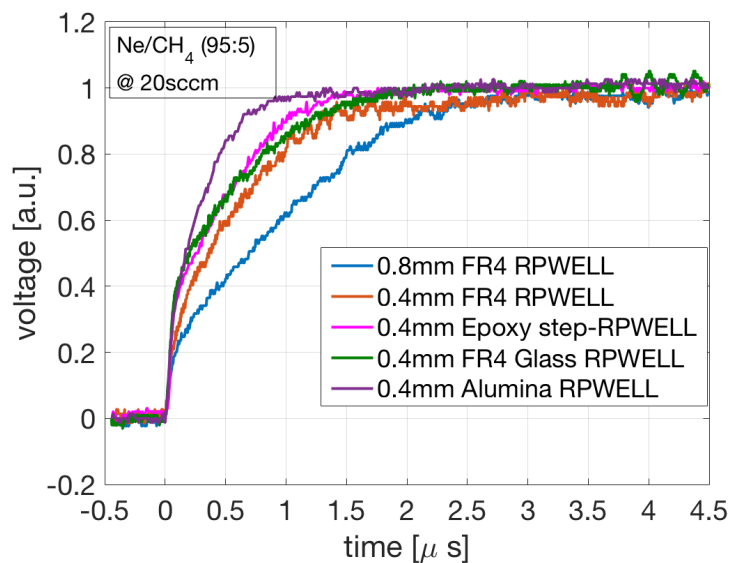


Figure 12: Normalized signal shape for the different RPWELL configurations; apart of the FR4 Glass RPWELL, the other configurations had Semitron resistive plates.

Figure 12 shows a comparison of the induced signals in different types of RPWELL detectors. The obtained signal shapes are consistent in their general shape; the rise times of the signal obtained with the 0.4 mm thick electrodes are of the order of 1 μ s (with an alumina electrode being slightly faster), while that of the 0.8 mm thick electrode is of the order of 2 μ s. This is expected since the rise time is dominated by the ion drift time which is double in 0.8 mm thick holes compared to that in 0.4 mm thick holes. In the different 0.4 mm thick electrodes, some variations are observed in the fast component of the signal induced by the electron movement - with that of the alumina THGEM, epoxy step-RPWELL and FR4 glass RPWELL having the largest fast-component fraction. This difference is not well understood and requires a more dedicated and systematic investigation of the different configurations signals.

2.5.2 Energy Spectra

All X-ray energy spectra shown in Figure 13 were taken during the gain measurements; in all cases the detectors were irradiated over an area of 3 mm². The 0.8 mm and the 0.4 mm FR4-made electrode with Semitron RPWELL yielded similar energy resolutions of ~19%-20% full width at half maximum (FWHM). The resolution values of the epoxy step-RPWELL, the alumina RPWELL and the 0.4 mm FR4 glass RPWELL were 21%, 19% and 22% FWHM - respectively; the THWELL resolution was ~18% FWHM.

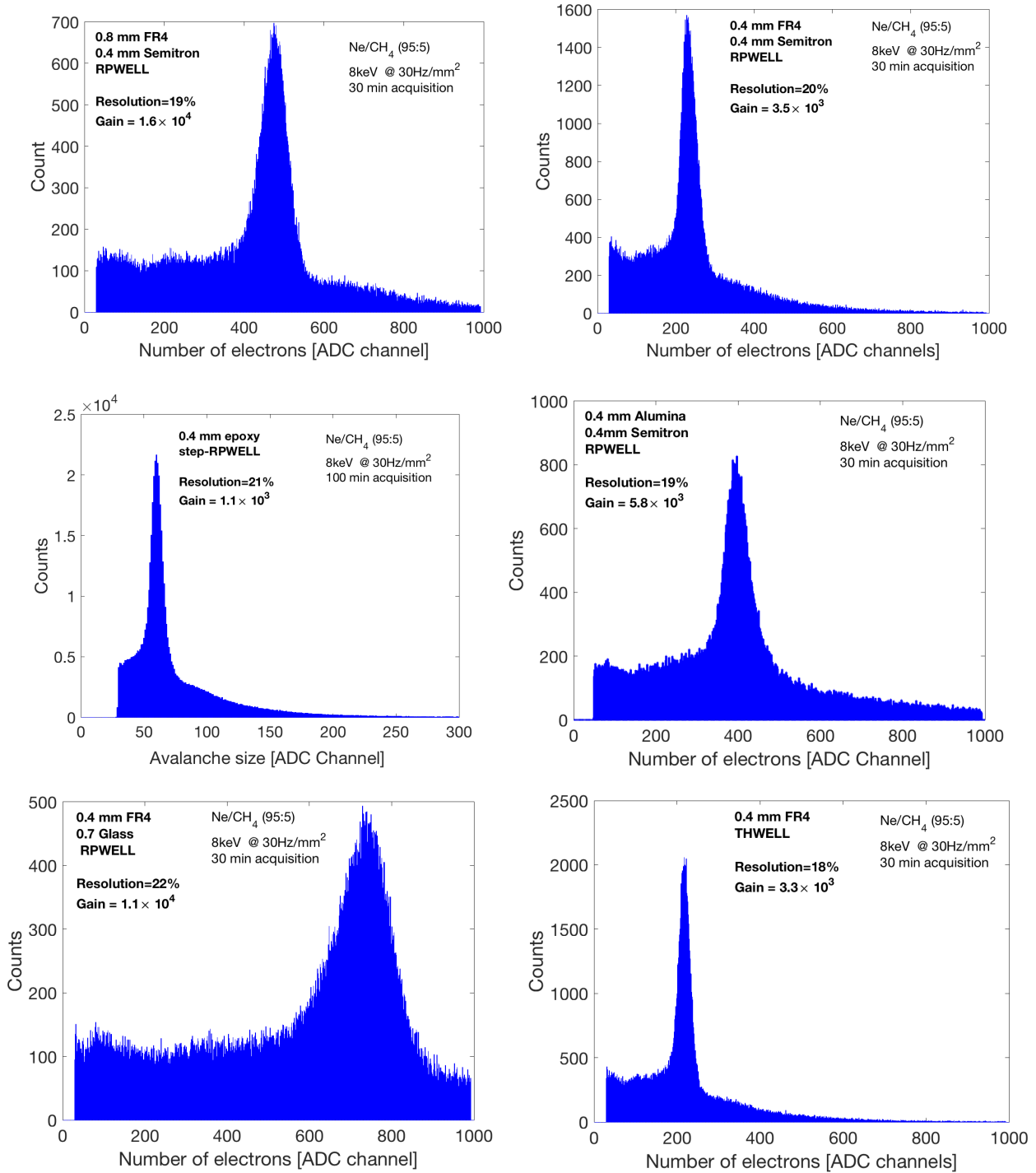


Figure 13: X-ray energy spectra of different configurations in Ne/CH₄ (95:5)

2.5.3 Gain Measurements

Figure 14 depicts the gain curves of the different detector configurations in Ne/CH₄ (95:5). The 0.8 mm and 0.4 mm FR4 RPWELL with Semitron reached similar maximal gains ($\sim 5 \times 10^4$). The 0.8 mm FR4 with 0.7 mm glass RPWELL and the epoxy step-RPWELL reached gains of $\sim 3 \times 10^4$ and $\sim 4 \times 10^4$, respectively. On the other hand, the alumina-WELL and the 0.4 mm FR4 with glass RP reached lower

maximal gains, while the THWELL had the lowest maximal gain.

Figure 15-Figure 20 present the gain variations with time, recorded along the gain-vs.-voltage measurements (as described in the section 2.4.2.1) in the different WELL configurations; shown are the values of the voltage and current supplied to the RPWELL Top electrode by the HV power supply. These plots demonstrate the necessity of addressing the stabilization time when characterizing the performance of an RPWELL detector. Furthermore, the role of the RP in suppressing discharges can also be seen: for the THWELL configuration (no RP – Figure 15) current spikes at the level of ~ 250 nA occur at 750 V. These discharges are accompanied by a gain drop of $\sim 80\%$. On the other hand, in the RPWELL detectors (Figures 16-20) the observed current spikes at the level of ~ 10 nA and these discharges are not associated with visible gain drops.

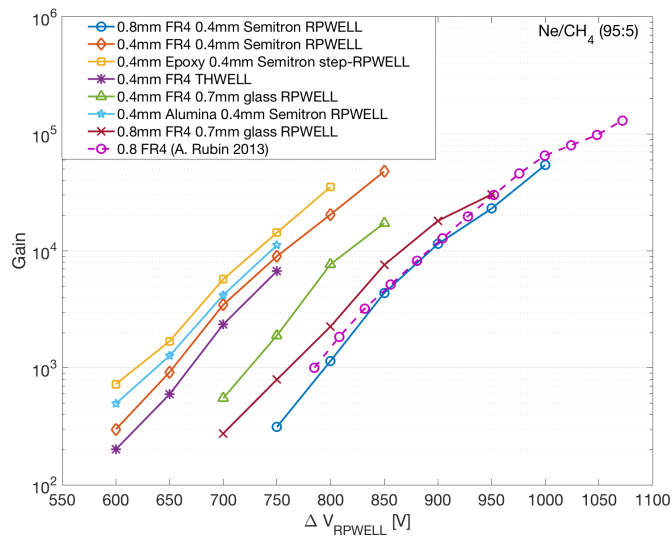


Figure 14: Gain vs. THGEM voltage of different RPWELL and THWELL configurations compared with Rubin's result [16]

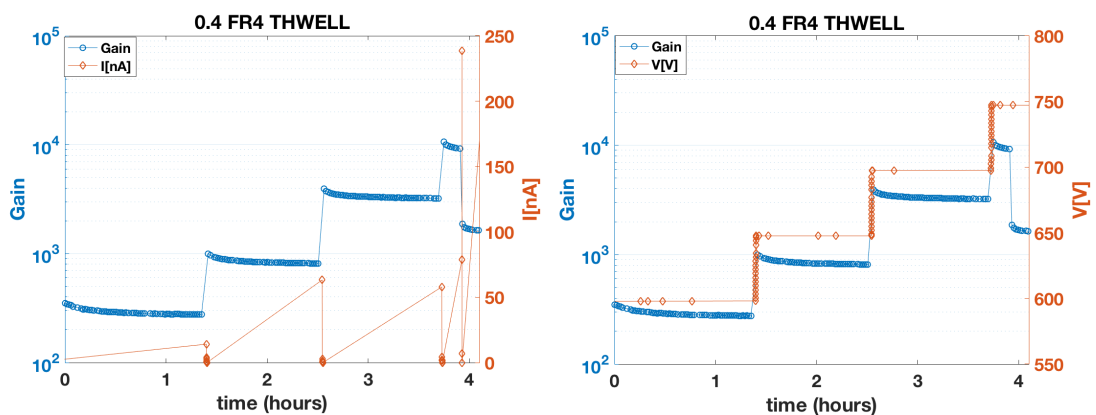


Figure 15: 0.4 mm FR4 THWELL - Gain measurement along with voltage (right) and current (left) monitors. Ne/CH₄ (95:5) at 20 sccm; 8 keV X-ray source @ ~ 30 Hz/mm².

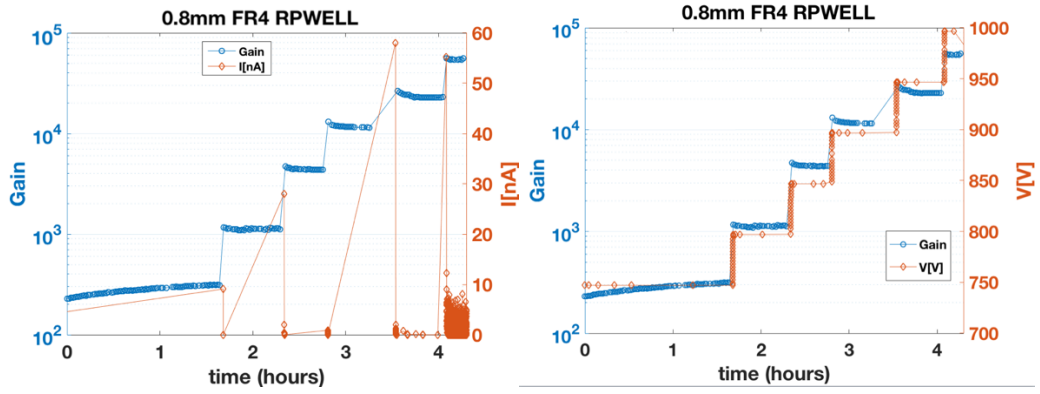


Figure 16: 0.8 mm FR4/0.4 mm Semitron RPWELL - Gain measurement along with voltage (right) and current (left) monitors. Ne/CH4 (95:5) at 20 sccm; 8 keV X-ray source @ ~30Hz/mm2.

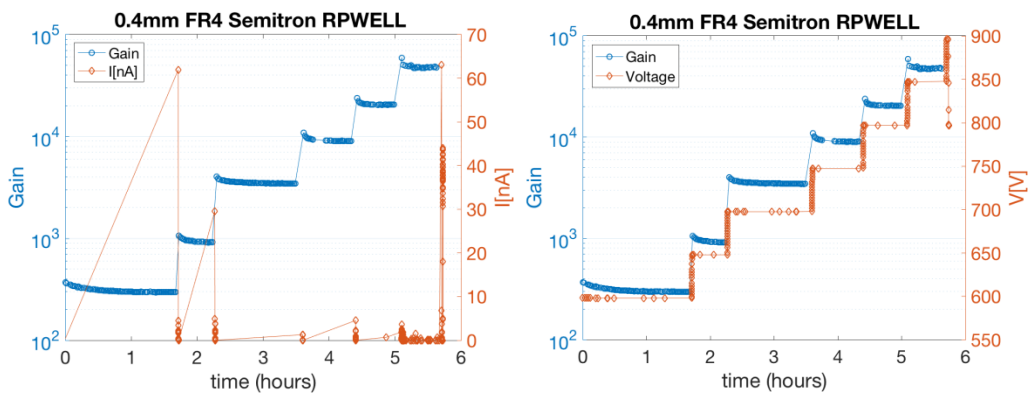


Figure 17: 0.4 mm FR4/0.4 mm Semitron RPWELL - Gain measurement along with voltage (right) and current (left) monitors. Ne/CH4 (95:5) at 20 sccm; 8 keV X-ray source @ ~30 Hz/mm2.

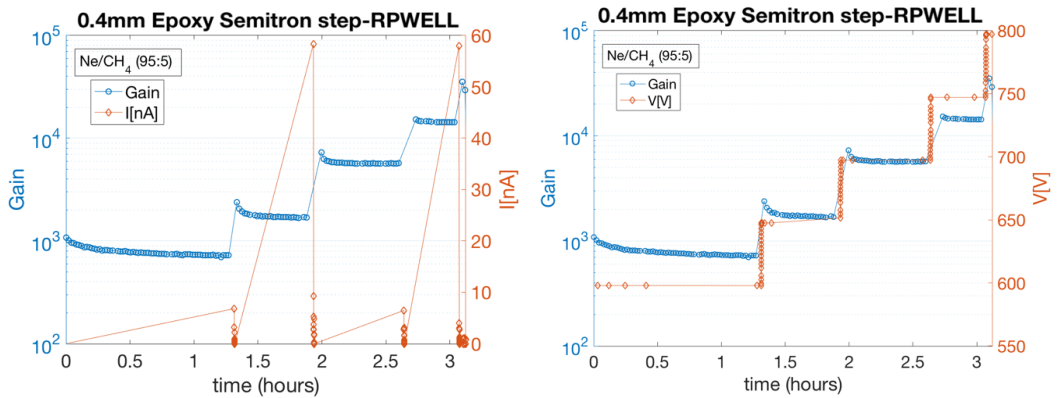


Figure 18: 0.4 mm Epoxy step-WELL/0.4 mm Semitron RP - Gain measurement along with voltage (right) and current (left) monitors. Ne/CH4 (95:5) at 20 sccm; 8 keV X-ray source @ ~30 Hz/mm2.

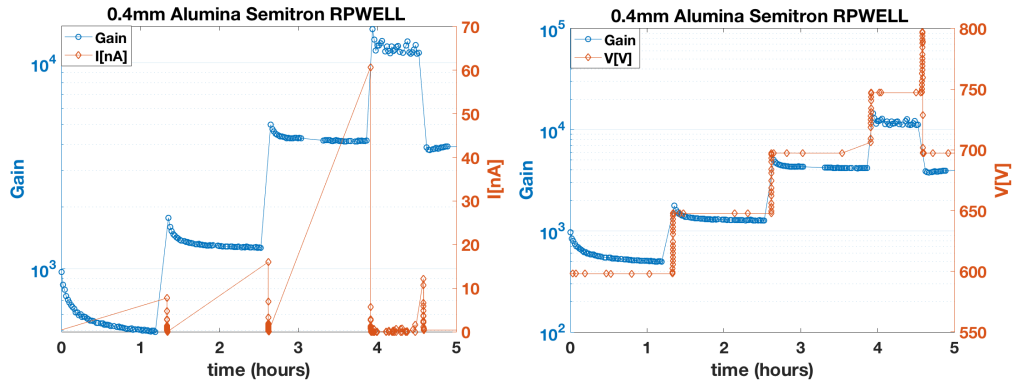


Figure 19: 0.4 mm Alumina/0.4 mm Semitron RPWELL - Gain measurement along with voltage (right) and current (left) monitors. Ne/CH4 (95:5) at 20 sccm; 8keV X-ray source @ ~30 Hz/mm2.

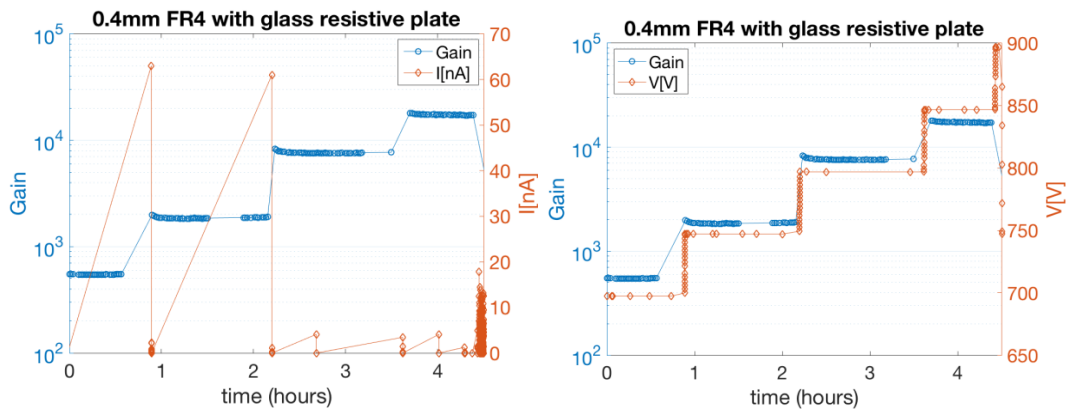


Figure 20: 0.4 mm FR4/0.7 mm LRS glass RPWELL - Gain measurement along with voltage (right) and current (left) monitors. Ne/CH4 (95:5) at 20 sccm; 8 keV X-ray source @ ~30 Hz/mm2.

2.5.4 Gain stabilization

A GSP measurement was performed on a 0.8 mm thick FR4 well with 0.7 mm thick LRS Glass RP in Ne/CH₄ (95:5). The initial preparations were in accordance with the Methodology for gain measurements. The voltage settings and the data acquisition were done according to Methodology for long term stabilization measurements (see section 2.4.2.2). The result is shown in Figure 21 (top). The gain stabilization was reached after 4 days. Moreover, in a time scale of one hour the gain reached a minimum and after two hours it started climbing (Figure 21 bottom left). A rate-dependency measurement followed (Figure 21 bottom right); raising the X-ray flux fortyfold, yielded first a 30% drop in the gain, succeeded by a two days long gain increase (by 29%). Then, when the rate returned to its initial value, the gain stabilized at a new value, higher by 20% than the one reached prior to the first increase in rate. The long (4 days) initial GSP witnessed in these measurements, motivated the improvement of the methodology of the initial preparations. The following measurements were conducted in accordance with the Methodology for long term stabilization measurements.

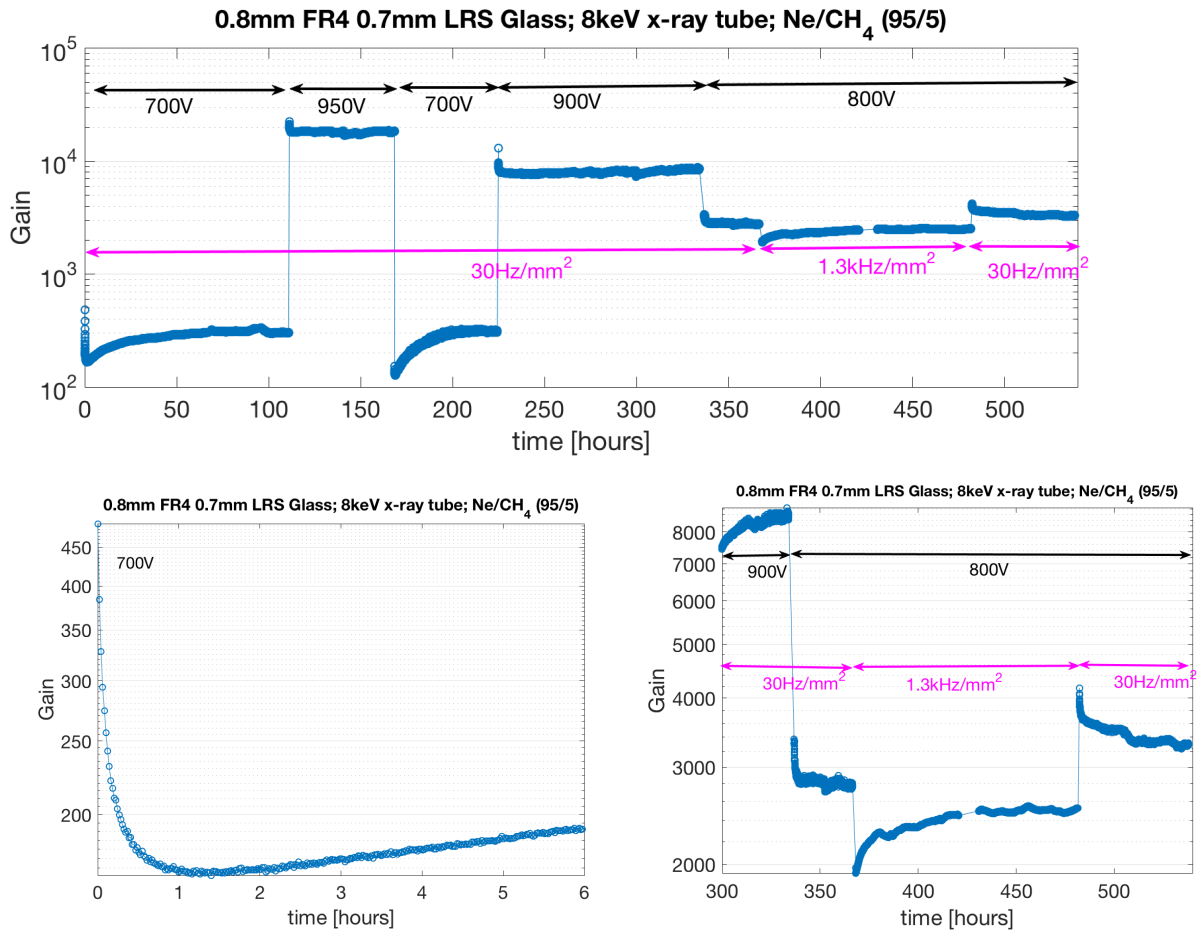


Figure 21: Typical gain stabilization process of 0.8 mm FR4 well with 0.7 mm LRS glass RP, after flushing the detector for only one 100 sccm hour. The top figure presents the full electrode history, while the bottom-left shows the first two hours of the GSP and the bottom-right shows a closer look on the rate dependency part of the measurement.

The presented GSPs in Figure 22 were recorded following the methodology described in section 2.4.2.2 as the voltage on the detectors' top electrode or the X-ray source flux (detector's count-rate) was changed. As can be seen, while the 0.4 mm electrodes initially stabilize within ~1 hour, the 0.8 mm RPWELL stabilizes only after four days. Figure 23 describes the GSP of a 0.8 mm RPWELL operated after the chamber was pumped and kept in 1.5×10^{-4} Torr for 24 hours and flushed for 24 hours with 20 sccm flow of Ne/CH₄ (95:5). In this process, the GSP was ended within two hours.

Figure 22-Figure 25 depict the GSP of the following configurations: 0.4 mm FR4 with Semitron RPWELL, 0.8 mm FR4 with Semitron RPWELL, 0.4 mm epoxy with Semitron step-RPWELL and 0.4 mm FR4 THWELL. The main observations are detailed bellow. A concise summary of these observations is given in tables 5 and 6. Note that the gain values obtained in these measurements are slightly lower than the gain values which were presented in the gain measurements (section 2.5.3), this is likely due to the fact that two different gas mixing methods were applied. The gain measurements were done using a pre-mixed gas and the stability measurements were done using a self-mixture.

Figure 22 shows that all three configurations, which underwent step 2 of the methodology (voltage cycle), returned to the initial gain after their operation voltage was returned to the initial value. Figure 24 presents a comparative view of this process for the 0.4 mm FR4 RPWELL and the 0.4 mm epoxy step-RPWELL. The initial stable gain of the RPWELL at 700 V was 1610 and when the top electrode voltage was increased to 850 V it raised to 1.9×10^4 , while the step-RPWELL yielded 1130 and 1.4×10^4 , respectively. When the voltage was reduced back to 700 V the RPWELL showed a 50% drop in gain compared to only 30% drop in the step-RPWELL. After 5 hours, the RPWELL gain recovered to 87% of the initial stable gain, while the step-RPWELL recovered to 96% of the initial gain. 15 hours later, the RPWELL gain was at 93% of the initial value.

	Initial stable gain @ $V_{top} = 700$ V	High gain @ $V_{top} = 850$ V	Time = 0 hours @ $V_{top} = 700$ V (relative to initial gain)	Time = 5 hours @ $V_{top} = 700$ V (relative to initial gain)	Time = 20 hours @ $V_{top} = 700$ V (relative to initial gain)
0.4 mm FR4 w/ Semitron	1610	1.9×10^4	804 (50%)	1400 (87%)	1510 (93%)
0.4 mm epoxy step w/ Semitron	1130	1.4×10^4	822 (72%)	1088 (96%)	1104 (97%)

Table 5: Summarized main observations of GSP due to operation voltage change, from 700 V to 800 V and back to 700 V (at time = 0) for 0.4 mm FR4 with Semitron RPWELL and 0.4 mm epoxy with Semitron step-RPWELL (extracted from Figure 24).

Exposed to source rate of 1.3 kHz/mm^2 the 0.4 mm thick RPWELL demonstrated a fast drop in the gain ($\sim 20\%$) followed by a gain-increase trend that lasted for ~ 10 hours. The detector's gain was stabilized at 106% of the initial stable gain, obtained at 30 Hz/mm^2 . A transition from 1.3 kHz/mm^2 to 30 Hz/mm^2 , concluded in a fast rise in gain followed by a slow decline which stabilized at a 130% of the initial gain. Repeating this rate transition cycle resulted in similar stable gain values for the lower and higher rates. The same trend was shown also with the 0.8 mm RPWELL except for ~ 2 days GSP at the first transition from low rate to high rate.

The epoxy step-RPWELL demonstrated a different behavior. Whenever the rate of 1.3 kHz/mm^2 was set, the gain dropped by $\sim 20\%$ and stabilized rapidly on a 15% of the initial stable gain; a return to 30 Hz/mm^2 resulted in a fast raise of $\sim 30\%$ and was stabled on 11% higher gain than the initial baseline gain.

Figure 25 presents a GSP of a 0.4 mm THWELL detector subjected to the same rate changes as described above. First it showed a fast stabilization of the order of less than an hour. When the rate was set for the first time to 1.3 kHz/mm^2 a GSP of 2 days was concluded at a gain value 41% higher than the stable gain measured at the lower rate. From this point, changing the rates from 1.3 kHz/mm^2 to 30 Hz/mm^2 didn't change the stable gain value. The fluctuations shown in the gain between the 100th hour to

the 250th one are correlated with room-temperature fluctuations and the time where the source was off in order to change the rates.

In addition to the GSP, Figure 22 shows that the 0.4 mm FR4 RPWELL suffers from gain drops in the presence of nano-discharges of more than 5 nA, while the gain of the 0.4 mm epoxy step-RPWELL remained stable even in the presence of 20 nA discharges. However, Figure 25 depicts that although the THWELL suffered micro-discharges of 0.2 μ A, there was no single visible gain drop correlated with them.

Detector configuration	Initial gain at 30 Hz/mm ²	Stable gain after 1 st transition to 1.3 kHz/mm ² (relative to initial)	Stable gain after 2 nd transition to 30 Hz/mm ² (relative to initial)	Stable gain after 2 nd transition to 1.3 kHz/mm ² (relative to initial)	Stable gain after 3 rd transition to 30 Hz/mm ² (relative to initial)
0.4 mm FR4 w/ Semitron	1610	1714 (106%)	2050 (127%)	1780 (110%)	2130 (132%)
0.8 mm FR4 w/ Semitron	1340	1405 (104%)	1654 (123%)	-	-
0.4 mm epoxy step w/ Semitron	1160	987 (85%)	1290 (111%)	1016 (87%)	1306 (112%)
0.4 mm FR4 w/o RP	1604	2264 (141%)	2256 (141%)	2265 (141%)	2252 (140%)
		1 st transition to 1.3k Hz/mm ² Immediate gain drop	1 st transition to 30 Hz/mm ² Immediate gain raise	2 nd transition to 1.3 kHz/mm ² Immediate gain drop	2 nd transition to 30 Hz/mm ² Immediate gain raise
0.4 mm FR4 w/ Semitron		20%	40%	25%	40%
0.8 mm FR4 w/ Semitron		15%	27%	-	-
0.4 mm epoxy step w/ Semitron		20%	27%	22%	30%

Table 6: Summarized main observations of GSP along two cycles of X-ray flux change, 30 Hz/mm² to 1.3 kHz/mm² and back to 30 Hz/mm², for 0.4 mm FR4 with Semitron RPWELL, 0.8 mm FR4 with Semitron RPWELL, 0.4 mm epoxy with Semitron step-RPWELL, 0.4 mm FR4 THWELL (no RP).

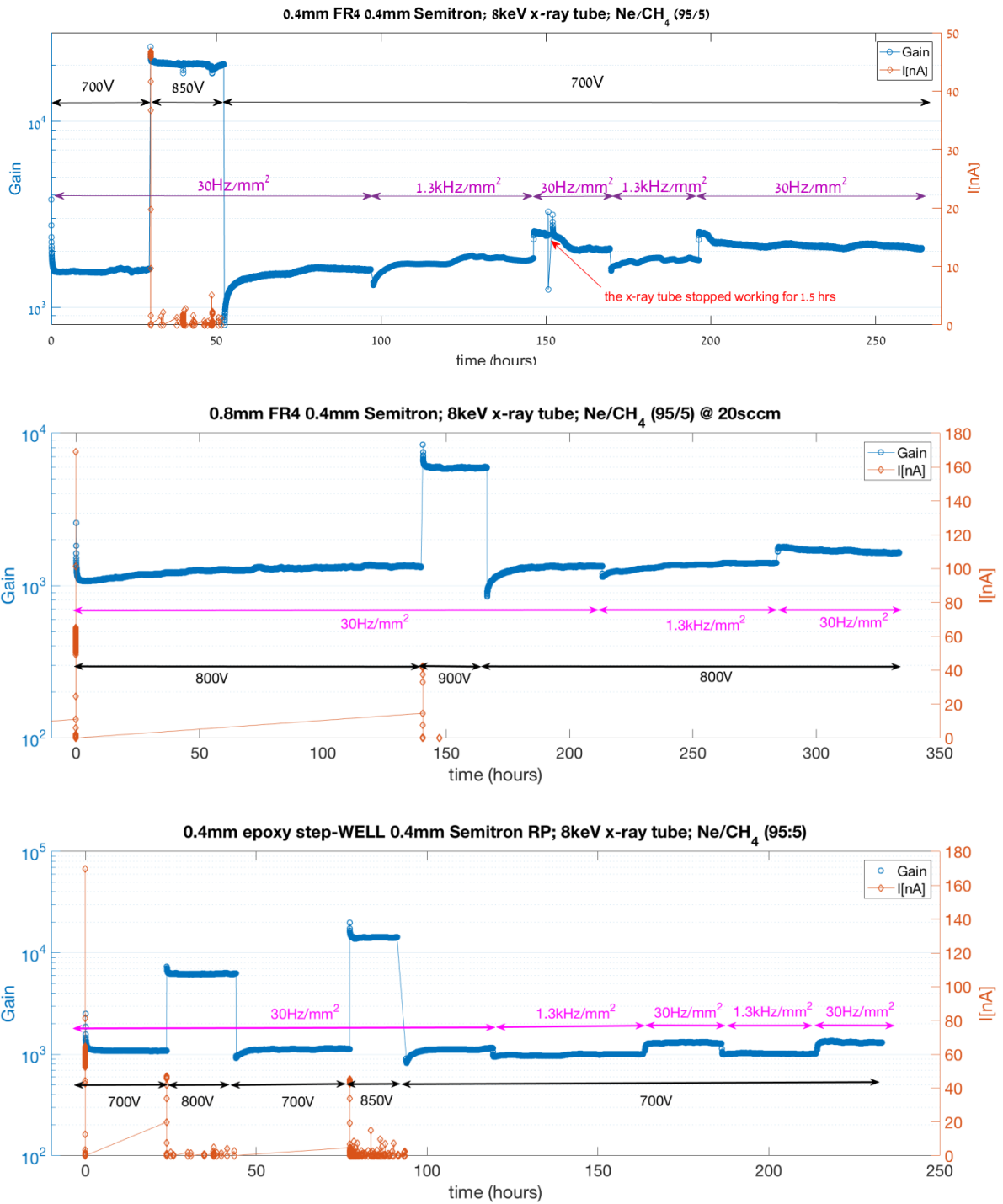


Figure 22: Typical gain stabilization processes of 0.4 mm (top) and 0.8 mm (middle) RPWELL and 0.4 mm epoxy step-RPWELL (bottom) in different (shown) voltages at the first period and at two X-ray rates – 30Hz/mm² and 1.3 kHz/mm². **NOTE:** at each increase of voltage the current from the power supply is registered – these are not discharges.

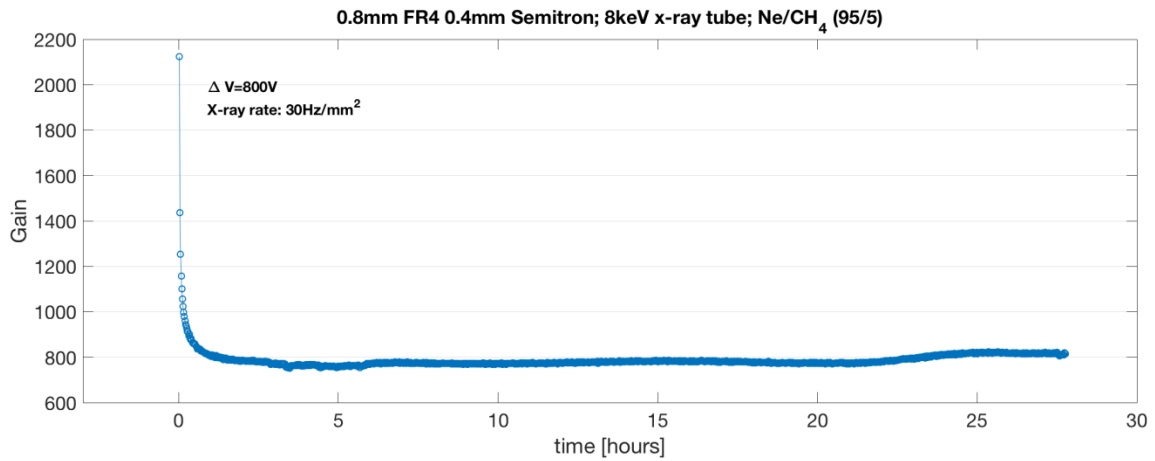


Figure 23: Typical gain stabilization process of 0.8 mm RPWELL taken after 24 hours in which the chamber was kept at 1.5×10^{-4} Torr and 24 hours along which the detector was flushed with 20 sccm Ne/CH₄ (95:5).

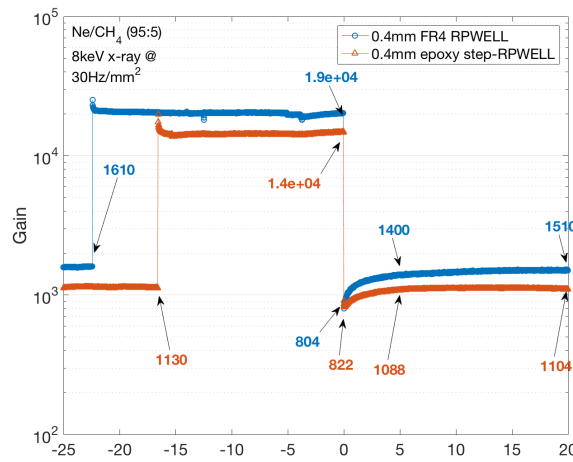


Figure 24: A comparison between the GSP of 0.4 mm FR4 RPWELL and the one of 0.4 mm epoxy step-RPWELL (Figure 22) when the gain is increased by an order of magnitude and reduced back, by changing the voltage on the top electrode from 700 V to 850 V and back to 700 V. We set time-zero to the beginning of the gain stability third process, after returning to the original voltage. The noted gain values are taken as follows: before increase of voltage, before returning to the original voltage and at time=0, 5, 20 hours.

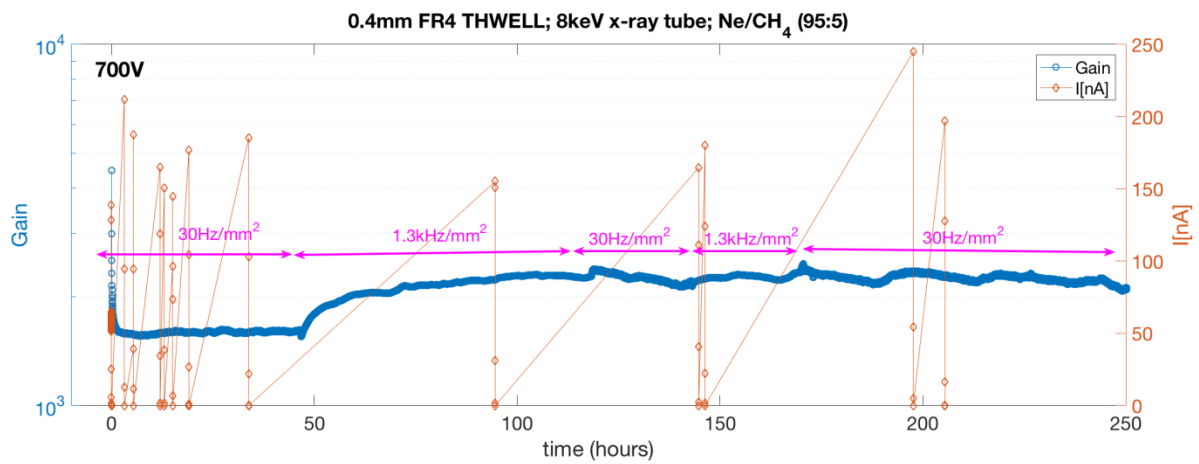


Figure 25: Typical gain stabilization process of 0.4 mm THWELL at two X-ray rates 30 Hz/mm² and 1.3 kHz/mm².

2.6 Discussion on section 2 results

2.6.1 Signal shape

The signal shapes measured with the various configurations are consistent in their general shape. The longer decay time observed throughout this work compared to that presented in [16] are attributed to the different readout chain used in the two measurements. In particular, in [16] the signals were recorded through a 200 kHz high-pass filter [17].

The signal rise time in the RPWELL detector consists of two main components; an initial fast component associated with the fast movement of the electrons towards the resistive plate and a slow component associated with the slow drift of the ions from the bottom of the hole towards the top electrode. As expected, the overall rise time of signals obtained in the 0.4 mm electrodes is about half than the one measured with the 0.8 mm electrode. This rise time is dominated by the slow ion component which is doubled in the thick electrode in which the ions drift along doubled length.

The relative fraction of the charge contained within the fast component varies between the various 0.4 mm configurations. This difference suggests that the fraction of charge contained in the fast component can be optimized, a possibility that could be important for applications requiring detection capabilities under high irradiation rates. The cause for this difference is not yet understood and should be investigated in a further study.

2.6.2 Energy resolution.

Using 8 KeV X-ray photons, the RPWELL configurations tested here (either with Semitron or LRS glass RP) yielded typical energy resolutions of 22-19% (FWHM); the THWELL (with no RP) yielded a resolution of 18% (FWHM). The resolution depends directly on the gain stabilization process. Note that no attempt was made to optimize the energy resolution throughout the measurements conducted in this study. It is not unlikely that better resolutions can be achieved with these detectors. Indeed, in a different set of measurements (not reported here) 18% (FWHM) resolution was obtained with a Glass RP.

2.6.3 Gain measurements

The gain curve measured with the reference detector (0.8 mm RPWELL) is consistent with that measured previously with another 0.8 mm RPWELL [16]. This strengthens the quality of the methodology applied.

The 0.8 mm thick and 0.4 mm thick FR4-based RPWELL detector with Semitron RP reached similar maximal gains. This is in agreement with Raether's conclusion that the avalanche size is the dominant parameter for the onset of discharges. The epoxy-based step-RPWELL reached maximal gain

similar to that of the two FR4-based detectors in spite of the presence of high field near the edges of the step, and in spite of the smaller rim around the holes. Compared to the 0.4 mm thick FR4-based RPWELL, similar gains were achieved at lower operation voltage. This is in agreement with the slightly higher field calculated in this configuration compared to standard RPWELL (Figure 5)

The maximal gain achieved with the 0.8 mm FR4 with glass RP was lower compared to that reached with the 0.8 mm FR4 Semitron RPWELL. The thinner (0.4 mm thick FR4) glass RPWELL demonstrated lower maximal gain than the thicker one. This could be attributed to 50 V steps that we used in the scan. The maximal gain of the thinner glass RPWELL showed no discharges (Figure 20) while the next step in voltage yielded ~ 20 nA discharges. Perhaps, a smaller step in the voltage would have brought gain to a limit closer to the discharge onset and result in the same maximal gain as the 0.8 mm FR4 glass RPWELL.

The alumina-based RPWELL presented poor performance. This is likely due to the production defects of the present electrodes with the weakest point being the small spikes inside the holes. Finally, as expected, the lowest maximal gain was that of the THWELL which lacks discharge-quenching mechanism.

On the other hand, when it was operated below maximum gain, the THWELL (Figure 25) suffered from discharges of two orders of magnitude larger amplitude than the ones of the 0.4 mm Semitron RPWELL (Figure 22 top); These discharges did not necessarily resulted in an observed gain drop. A follow-up study should be performed in order to systematically define a discharge and its effects on the detector performance. Currently, the maximal gain is defined by the onset of nA current activity; we did not study though their effect, e.g. the possible dead-time induced and the area affected in the discharge neighborhood.

2.6.4 Gain stabilization

Gain stabilization at increasing operation voltage can be assessed from Figure 16-Figure 20. Typically, an increase in the operation voltage of the RPWELL results in an immediate significant rise in the gain, followed by a slower decline (10-50%, depends on the size of the voltage increase) to reach stabilization (decay time of the order of 40 minutes – depends on the magnitude of the voltage step). This behavior can be explained by charging up effects: at higher voltage, more charge is produced in each avalanche and with time, more charge reaches the walls of the hole. The hypothesis that this behavior is related to the presence of the resistive plate is not supported by the fact that similar behavior was obtained also with the THWELL and was witnessed also in regular THGEM [33,42].

Note that the gain profile measured with the 0.8 mm FR4 with Semitron RPWELL (Figure 16) does not demonstrate an incline in the gain when the voltage was ramped up from zero to 750 V. This

inconsistency does not contradict the above conclusions since in this particular measurement the detector was not brought to the same initial conditions (as discussed in section 2.4.2.2) and the measurement was conducted after the detector was operated at a higher gain. The apparent increase of the gain can be explained by a process opposite to the charging up process discussed above; the high charge might be evacuated from the holes. This inconsistency was the main incentive to improve our method of equalizing electrode initial conditions.

In what follows, we discuss the results of the long-term stabilization measurement presented in Figure 21 to 25. Following the methodology described in section 2.4.2.2, we discuss our observations in the three measurement steps:

Step 1: Initial gain stabilization

Step 2: Gain stabilization in the transition between low and high operation voltages at low irradiation rate

Step 3: Gain stabilization in the transition between low and high rate at constant operation voltage

Initial gain stabilization: As discussed above, once the voltage was first ramped up, the gain increased over a short time scale and then slowly decreased. From Figure 26 in which a zoom into the first two-hours region is shown, it seems that after ~ 1 hour the gain stabilizes. This was the ground to the methodology upon which the gain-vs.-voltage methodology was based. However, as can be seen in Figure 21 time scale at the order of 2 hours is insufficient and a rise of 75% of the gain was observed in the following days.

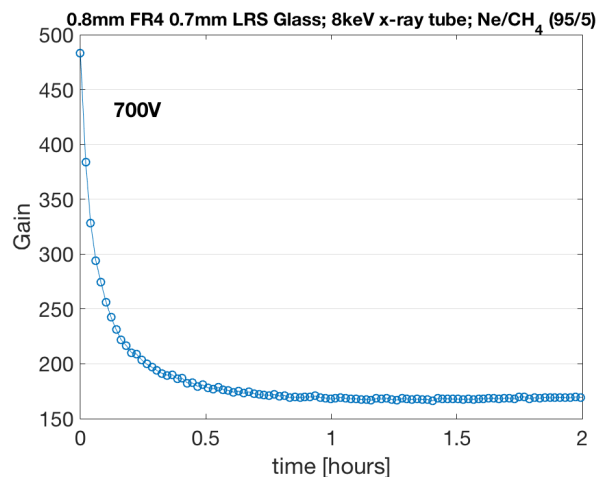


Figure 26: The first two hours of the GSP of a 0.8 mm thick FR4 WELL with 0.7 mm thick LRS glass RP as presented in Figure 21.

The long time-scale needed for gain stabilization suggested that outgassing from the electrodes (for example humidity absorbed in the detector elements when it was exposed to air prior to the assembly) could be affecting the measurements. This assumption is supported by the following observations: 1) No long-term increase in the gain is observed when switching on the voltage after 4 days

of constant flushing with HV off (see Figure 22 and Figure 25). Hence, this stabilization is not related to changes in electric properties. 2) The long-term stabilization of the 0.8 mm electrode is much longer than that of the 0.4 mm electrode (4 days of HV off and 4 days of HV on, compared to only 4 days of HV off, Figure 22). Indeed, more outgassing is expected when using thicker materials. 3) The long-term stabilization time of an RPWELL with glass RP is shorter than that of Semitron RP. This is consistent with the fact that Semitron is known to absorb water while the glass does not absorb water. 4) When pumping the detector (0.8 mm electrode with Semitron) for 24 hours prior to its operation, the stabilization time was reduced significantly (Figure 23).

This phenomenon, where the gain is increased during first stabilization process, was also reported in [33] where the increase trend of the gain was attributed to the charge movement in the PCB fiberglass plates when the THGEM electrodes reach high electric fields; since the displacement of charge inside the insulator bulk is slow, the time scale for stabilization can be in the order of hours or even days. The results presented in this work do not support this assumption.

Gain stabilization in the transition between low and high operation voltages at low irradiation rate:

As discussed in detail earlier, the transition from low to high operation voltage is characterized by an immediate increase in the gain which is followed by a slower decrease (time scale of an hour). This is in agreement with the assumption that the detector charges up until it reach a steady state. The transition from high- to low operation voltage is characterized by an immediate sharp drop in the gain which is followed by a slower increase in the gain (time scale of a few hours). Note that the time scale related to the gain stabilization after increasing the gain is much shorter than the time scale related to the gain stabilization after reducing the gain. This suggests that different physics processes dominate in each of these operations. One possible explanation could be that when ramping up the voltage, the avalanche size increases and more electrons and ions attach to the walls of the holes. However, when decreasing the voltage, the dominant effect is the charge evacuation from the walls of the holes which is slower in nature. These results strengthen the charge-equilibrium model, which claims that the higher the space-charge in the holes, the higher the charge accumulation on the insulator [32,40].

Another observation is that after stabilization, the application of the same operation voltage results in the same gain. Hence, in the conditions that were tested, the increase and then decrease of the gain did not change the steady state of the detector.

In addition, we see that the 0.4 mm FR4 RPWELL was more affected by the exposure to higher space-charge, than the epoxy step-RPWELL. The former suffered from a larger relative drop in the gain and longer time was required until it regained stability at the initial voltage than the latter. In order to deduce whether the first detector suffered from more charge up (geometry related effect) or from slower

charge evacuation process (mainly material related), a future more elaborated comparison between epoxy-made regular-RPWELL and step-RPWELL will be performed.

Stabilization in the transition between low- and high irradiation rates at low gain: Assuming once again the charge-equilibrium model, the expectation was that an increase of space-charge by increasing the rate of the avalanches occurrence will reduce the gain. This was shown in previous RPWELL studies [16,24-26] which explained their results based upon this model.

The measurements presented here depict a different behavior; the first transition from low rate to high rate, resulted in an immediate gain drop (less than a minute – one spectrum acquisition), which was followed by slow increase in the gain (more than a day); the gain was finally stabilized at a value closer to the one measured at the low rate. When the rate was lowered again, the original gain was not restored. The gain at the steady state was changed and stabilized at a higher value.

This observed behavior is counterintuitive and requires further studies. Based on the studies we have conducted we can draw the following conclusions:

- The stabilization effect is not related to the resistive plate as it is also observed with a bare THWELL configuration.
- This effect is reduced in the step-RPWELL configuration suggesting that it is related to charges accumulating on the walls of the holes. Since the step-RPWELL is made of epoxy it could also be that the difference is due to difference between the two materials.
- Once the new conditions are established, additional dependencies of the gain on the irradiation rate are related to the RP. While a gain drop at the higher rate was demonstrated by both RPWELL and step-RPWELL detectors, no such drop was detected with the THWELL (at the rates that were tested).

2.7 Conclusions

A survey of different RPWELL production techniques – mechanical drilling, laser cutting and photo-lithography – and different materials - FR4, Epoxy, Alumina, Semitron and low-resistive silicate glass have been carried out. While FR4-based RPWELL performs well, the epoxy-based RPWELL showed equal gain capabilities and less sensitivity to variations in the irradiation rate. The performance in terms of maximal achievable gain and stability of alumina-based RPWELL tested in this work was worse compared to the other detectors. This is likely due to the poor production quality, in particular the sharp residual edges created by the laser drilling process - which will have to be improved.

An RPWELL with a new resistive-plate material, the low-resistive silicate glass (bulk resistivity of 10^{10} Ωcm [37]) was investigated. The glass-RPWELL, with the advantage of absorbing less humidity

and expanding less with temperature, was stable at high operation gains and under high irradiation rates, making it a promising solution for future detectors. RPWELL detectors with other resistive materials, such as ceramic (10^9 - 10^{10}) [43,44] and Tivar[®] ESD (bulk resistivity of 10^7 - 10^8 Ωcm) [45], will be tested in the future.

The high-resolution photolithography production technique of epoxy electrodes permits conceiving electrodes with more complex geometry. E.g. the resulting step-hole electrode provided us with an additional tool for investigations of charging-up effects.

Gain stabilization in response to change of operation voltage (and gain) and change of irradiation rates were assessed. While the response of the RPWELL to abrupt variation in operation voltage met our expectations, unexpected response has been observed when the irradiation rate was changed. In particular, in the transition between low- and high-rate, the detector gain underwent a change (likely related to charging up of the walls of the hole) that was not restored when the irradiation rate was reduced. This behavior was less pronounced with the epoxy-based step-RPWELL, suggesting that the rate dependency can be mitigated. Moreover, the fact that after the first cycle of rate change no additional changes of the gain of the THWELL were observed provides us with an incentive to study the effects of RP materials with lower bulk resistivity, such as the Tivar.

Future studies include long-term stabilization studies also with an epoxy-based RPWELL, to rule out the possibility that the different response to changes in the rate between the FR4-based RPWELLS and the epoxy-based step-RPWELL are related to the materials (FR4 vs. epoxy) and not the geometry.

An important outcome of this study is the development of a robust methodology for the characterization of THGEM-based detectors. The results of this study were found reproducible; they provided a good insight into the phenomenology of RPWELL operation, that will allow investigating more systematically and accurately the physics processes governing their response. The methodology is certainly applicable to other types of gas-avalanche detectors.

3 First characterization of UV-photon detection in RPWELL-based detectors

3.1 Introduction

UV-photon detection has various applications from particle identification using Ring Imaging Cherenkov (RICH) single-photon detectors [2,46], to scintillation-light imaging in radiography [8], medical imaging [47] and rare-events searches with noble-liquid detectors [48] (multiple photons). Besides vacuum Photo-Multiplier Tubes (PMTs), Gaseous Photomultipliers (GPM) [49] have been playing an important role, particularly for RICH; detectors employed were Wire Chambers [50], cascaded GEMs [51] and lately THGEM-based GPMs [52].

The single-photon detection efficiency relates to the quantum efficiency (QE) of the photocathode which depends on the wavelength, λ , of the photon and on the efficiency of detecting the resulting photoelectron. The effective photon detection efficiency (PDE or ε_{eff}) of a GPM detector is therefore:

$$\varepsilon_{eff}(\lambda) = QE(\lambda)A_{eff}\varepsilon_{extr}\varepsilon_{coll}\varepsilon_{thresh} \quad (11)$$

A_{eff} is the fraction of electrode surface covered with the reflective coating. ε_{extr} is the photoelectron extraction efficiency into the gas. ε_{coll} is the efficiency to collect the extracted electrons into the holes. ε_{extr} and ε_{coll} are hard to decouple in a measurement, both depend on the gas mixture, applied electric field and electrode geometry. ε_{thresh} is the probability of a signal to be above a given threshold.

In single-photoelectron detection, ε_{thresh} is strongly related to the shape of the pulse height spectrum. This spectrum reflects the physical processes governing single-electron avalanche multiplication. As explained in section 1.1.4, in case of an exponential avalanche distribution, high detection efficiency of single-photoelectrons can only be achieved if the mean avalanche size is high. Otherwise, for any given threshold (set above noise), a large fraction of the events will be below threshold. Therefore, there is a clear advantage for detectors that can be operated in a Polya regime [53]. In particular, if the Polya peak is significantly above the threshold.

While Polya distributions were demonstrated in some MWPCs [54,55], they were reached only with a few MPGD-based detectors [56,57].

In this study two RPWELL-based photon detectors were evaluated: the first was a CsI-RPWELL - a single-stage FR4-based RPWELL with Semitron resistive plate in which the top electrode was coated with cesium-iodide (CsI). The second was a dual-stage detector consisting of CsI-THGEM followed by a transfer gap and a standard copper clad FR4-based RPWELL with Semitron resistive plate.

We present a first evaluation study of these two photon-detector prototypes, in terms of potential gain in PDE. A discharge-free operation in the Polya regime was demonstrated in both; trends of the gain in PDE as function of the Polya parameter θ (as defined in section 1.1.4 equation 5) are Shown.

3.2 Apparatus & Methodology

3.2.1 Experimental setup

The experimental setup is shown in Figure 27. It consisted of UV- and X-ray sources, a vessel containing the examined detector and a readout system.

In these experiments, we used a H₂ discharge lamp UV-source and an Fe⁵⁵ X-ray source. The H₂ discharge lamp yields pulsed emission; the rate of the pulses was controlled by the voltage supplied to the lamp – up to 4 kV. In this experiment, the lamp was operated at 3.7 kV, supplied by a “dual MWPC power supply” model 6900. The UV intensity was heavily attenuated using Oriol UV neutral density filters (2.4 dB) and by distancing the source from the detector until a rate of ~ 1 Hz/mm² was observed.

The detector vessel was flushed continuously with a gas mixture of Ne/CH₄ (95:5) mixed using a MKS 247D four-channel readout for monitoring and control of the gases mass flow. The detector vessel had two windows – a Kapton one for the X-ray photons and a quartz one for the UV.

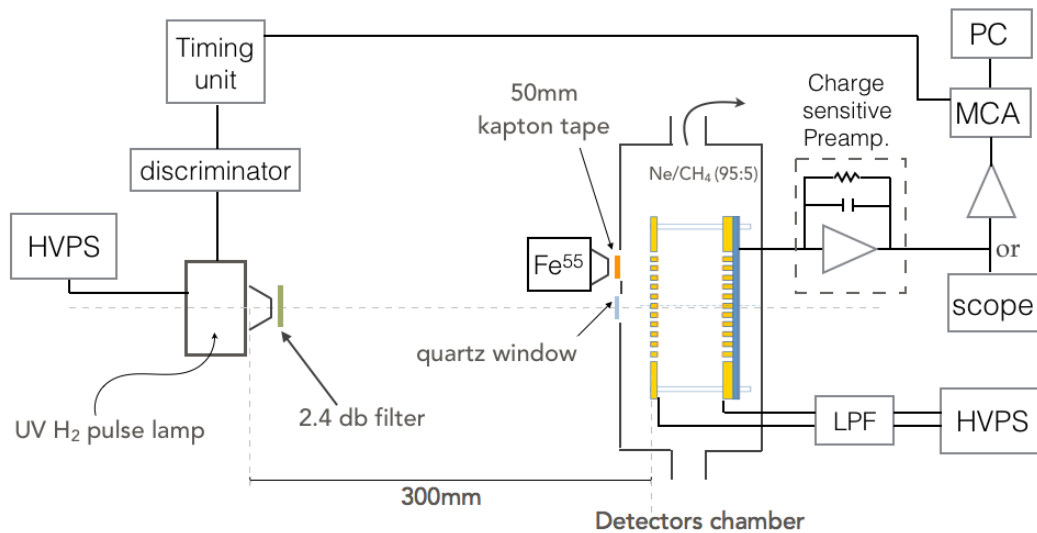


Figure 27: Experimental setup for the UV detector investigations using a UV lamp and a Fe⁵⁵ X-ray source.

The two studied 30×30 mm² RPWELL-based configurations are depicted in Figure 28. The base structure RPWELL comprises 0.4 mm thick single-sided Cu-clad FR4 THGEM (Top) pressed to a 0.4 mm Semitron® ESD225 painted on the bottom side with carbon glue (~ 1 k Ω /□) and coupled to a readout anode using 3M™ Electrically Conductive Adhesive Transfer Tape 9707. The single-stage detector (CsI-RPWELL) is a typical RPWELL with CsI photocathode (~ 500 nm thick) evaporated on its top face, preceded by a 10 mm drift gap and a drift cathode (here we simply used a 0.4 mm single-sided THGEM facing towards the RPWELL). The second detector had a dual-stage structure with a CsI-coated 0.4 mm thick double-sided FR4 THGEM, followed, after a 2 mm transfer gap, by a standard RPWELL stage (Cu-

RPWELL). In the last configuration, a field of 0.5 kV/cm was applied across the transfer gap; A 700 V voltage difference was set across the THGEM electrode for optimal UV-photoelectron collection efficiency [5].

Two main modes of HV configurations were used: with and without drift field. Based on previous experience [49], UV photons were detected with no drift above the photocathode. The detection of soft X-ray photons was carried out with a 0.5 kV/cm drift field, enabling the collection of the primary electrons. The power to the detector electrodes was supplied via low-pass filter (LPF) using CAEN A1651H module and SY5527 mainframe; the current and voltage monitoring was done with the CAEN GECO2020 software.

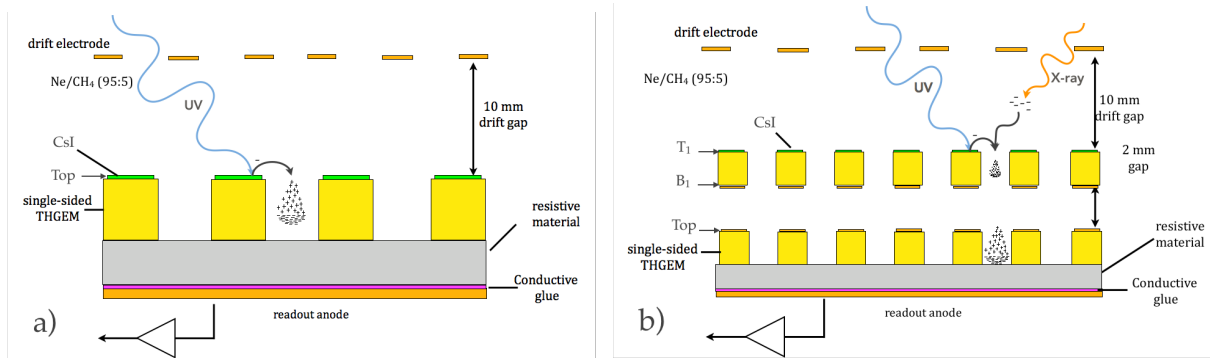


Figure 28: Two UV-detector configurations: a) 0.4 mm FR4/0.4 mm ESD225 Semitron CsI-coated RPWELL (CsI-RPWELL); b) dual-stage detector with a CsI-coated 0.4 mm double-sided THGEM followed by a standard Cu-clad RPWELL (Cu-RPWELL).

The readout system was also operated in two modes – triggered and non-triggered. The signals were recorded from the anode through CAEN A1422 charge sensitive preamplifier by either the oscilloscope, for signal shape acquisition, or by a multi-channel analyzer (MCA) through an Ortec 572A linear amplifier with 2 μ s shaping time, for spectra acquisition. The signals were acquired by the MCA in triggered or non-triggered mode – for the X-ray and UV sources, respectively. To ensure counting only single-photon events, the rate of the UV pulsed lamp, after the filter, was set to have a single UV signal on the detector for every 10 trigger signals. Every discharge in the H₂ pulsed lamp resulted in a pickup signal; it was processed by a LeCroy 623B octal discriminator and then transferred to the coincidence gate input of the MCA through a CAEN 2255B dual-timer; the latter delayed the signal and expanded its time duration to allow the shaped detector signal processed by the linear amplifier to be counted.

3.2.2 Methodology

In section 2.4.2 we presented a methodology for RPWELL characterization, coping with instabilities due the charging-up of its insulator materials. This methodology could not be adapted for the study of a detector with a CsI photocathode; these have a surface resistivity in the $10^{11} \Omega/\square$ range [58].

They are sensitive to moisture in air – which did not allow for charge evacuation through air and the use of the electrostatic gun – that could harm the QE of the photocathode. Therefore, the reported detector gain values presented in this study could vary within $\sim 50\%$ - the maximal previously observed gain drop due to charging-up effects (section 2.5.4). In addition, long stabilization processes could affect the shape of the acquired spectra, thus the accuracy of the extracted values of the Polya parameter θ .

The analogue-to-digital converter (ADC) of the MCA was set to a range of 10 V divided to 1024 channels. The readout chain was calibrated using the standard calibration circuit depicted in Figure 29. For each coarse amplification of the linear amplifier, a new calibration was performed. A square wave signal was generated using the Agilent technologies InfiniiVision DSO-X 3034A oscilloscope's wave generator. Its $50\ \Omega$ impedance output was connected to the oscilloscope $50\ \Omega$ impedance input for a reading of the generated wave amplitude ($V_{calibrate}$) and to the preamplifier either by the test input ($C_{calibrate} = 1\text{pF}$) or through an external RC box ($C_{calibrate} = 7\text{pF}$) for the lower coarse gains. The connected capacitor would release a charge of $Q_{calibrate} = V_{calibrate} \cdot C_{calibrate}$ to the preamplifier and the rest of the readout chain. Finally, a linear fit was conducted to the number of electrons ($n_e = Q_{calibrated}/q_e$; $q_e = 1.6 \times 10^{-19}\text{ C}$) as function of the corresponding ADC channel.

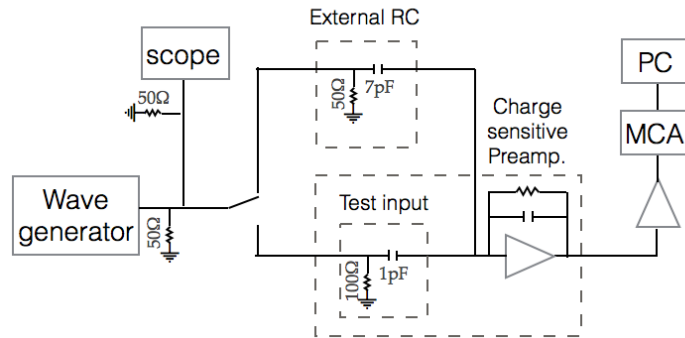


Figure 29: Calibration scheme.

The measurements were done in the following way. For each detector configuration, a gain curve was recorded. At each RPWELL operation voltage, several spectra were acquired, over 120 seconds each, in order to obtain enough statistics. A sum of the UV spectra per voltage value was fitted to a Polya distribution function, described in equation (5), while weighting each point with the square root of the ADC-channel counts. The gain was extracted using the system calibration method described above, where the number of electrons in a single-electron avalanche is its gain. The Fe^{55} spectra, recorded for each voltage value, were fitted to a Gaussian distribution and the gain was calculated as the corresponding number of electrons divided by the number of primary electron-ion pairs deposited by a

5.9 keV photon in the detector drift gap (eq. 2), $Gain_{Fe^{55}}(Ne - 5\%CH_4) = /164$. Each voltage scan ended at the onset of logged current spikes of a few nA (nano-discharges) on the detector electrodes.

The dual-stage detector was studied under both UV and X-ray sources in two drift field modes. The first voltage scan was done using the UV source without drift field, the second was done with the X-rays in drift mode and the last set was done again using the UV lamp without drift field.

3.3 Results

Figure 30 shows the typical single-photon pulse-height distributions (vs normalized detector gain) of the two detector configurations (Figure 28). As can be seen, in the two configurations Polya distributions were obtained. The fitted Polya parameters of the CsI-RPWELL are $\theta=0.3$ and an average gain of 1.5×10^5 and for the dual-stage detector $\theta=0.32$ and an average gain of 10^6 . Figure 31 exhibits the similarity of the spectra obtained in the different configurations operating at similar gains.

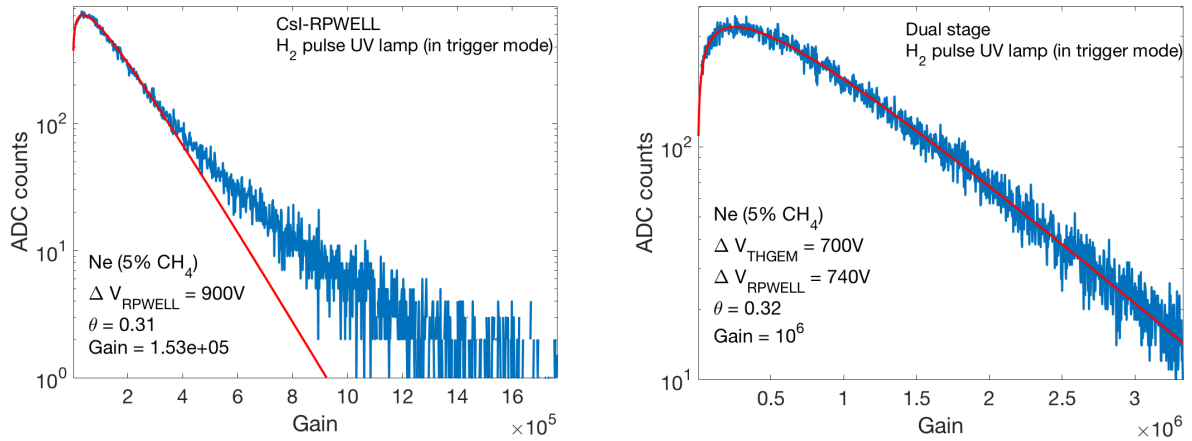


Figure 30: Typical UV spectra of the two configurations of Figure 28 recorded with the H₂ pulsed lamp in trigger mode. CsI-RPWELL (left); Dual-stage (right).

Figure 32 shows the trend of θ versus the RPWELL voltage and the achieved gain. The extracted θ -values are between zero to 0.35. It is observed that the Polya parameter is increasing with the voltage and the gain.

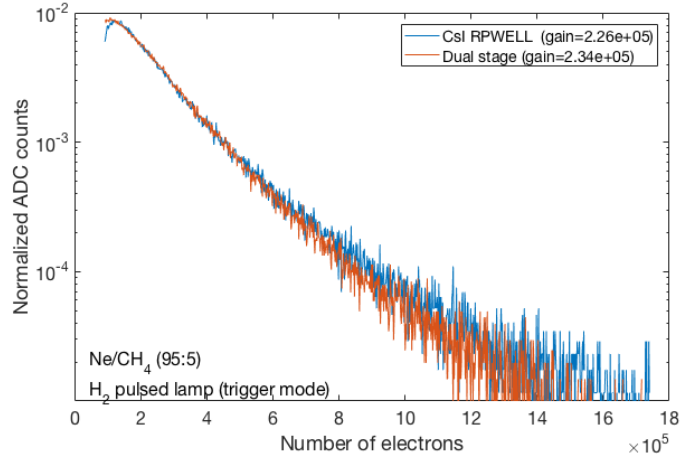


Figure 31: Pulse height distribution of the two configurations at a gain of $\sim 2.3 \times 10^5$.

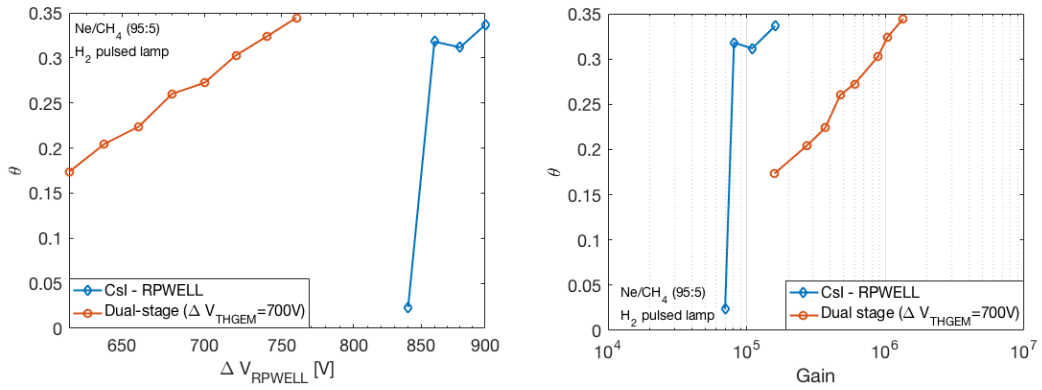


Figure 32: The Polya distribution parameter θ as function of the voltage applied on the RPWELL stage (left) and the gain (right)

In Figure 33 we present the gain versus the voltage applied on the RPWELL stage. The single-stage configuration yielded maximal gain of $\sim 1.5 \times 10^5$, while the Dual-stage one reached a maximal gain of $\sim 1.5 \times 10^6$.

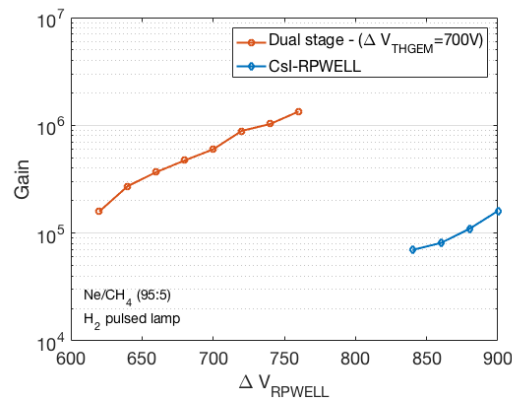


Figure 33: Gain as function of the voltage applied on the RPWELL.

Figure 34 shows three gain-curves of consecutive measurements of the dual-stage according to the methodology mentioned in the last paragraph of section 3.2.2. These results show the detector

performance in two operation modes and two types of sources, i.e. different avalanche size. It shows that the gain with the Fe^{55} X-ray source in the dual-stage detector with drift field is lower by about an order of magnitude than the gain obtained with the UV source in the first measurement. Furthermore, the maximal gain obtained with the X-ray source was $\sim 2 \times 10^5$. The maximal gain with the UV was about the same in both measurements, while the corresponding voltage was different.

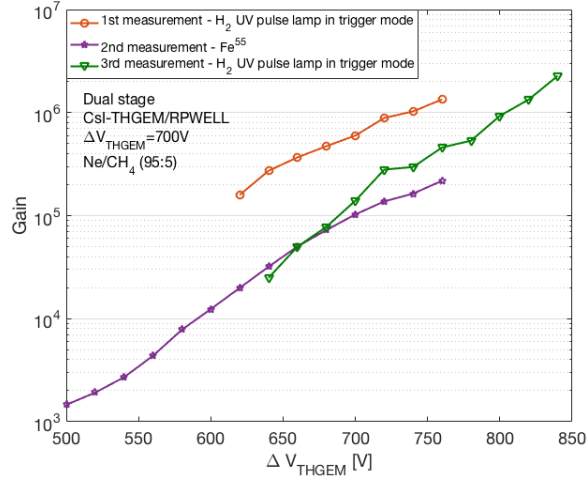


Figure 34: Dual-stage gain curve for three consecutive measurements. 1) H₂ lamp in trigger mode with zero drift field; 2) Fe⁵⁵ with 0.5 kV/cm drift field; 3) H₂ lamp in trigger mode with zero drift field.

3.4 Discussion on section 3 results

Two RPWELL-based detectors were investigated in Ne/CH₄ (95:5) using a H₂ discharge lamp as UV source and Fe⁵⁵ as 5.9 keV X-ray source: a single-stage CsI-RPWELL and double-stage, CsI-THGEM + Cu-RPWELL. Clear Polya charge distributions for single photons were demonstrated in both configurations. The θ parameter of the various Polya distributions, extracted from the data fitting the distributions, was between 0.2-0.35 with peaked spectra above the ADC threshold (channel no. 4 out of 1024). As mentioned above, higher value of θ indicates better separation of the Polya distribution from noise with a resulting better signal-to-noise separation. Hence higher θ values indicate potentially higher detection efficiency. Indeed, higher θ values were obtained at higher gains (Figure 32).

Both RPWELL-based UV detectors demonstrated a discharge-free operation at a gain of 10^5 for single-stage and 10^6 for the dual-stage detector.

The effect of exposure to high radiation was assessed by irradiating the double-stage detector, in addition to the UV, with an Fe⁵⁵ X-ray source; the same maximal achievable gain was reached before and after the exposure to high radiation, however, at different operation voltage. This proves that the onset of discharges depends on the gain (as predicted by the Raether's limit) and not on the applied voltage.

The dual-stage detector was operated stably at a gain of 2×10^5 also under irradiation with Fe^{55} X-ray photons. The average charge induced by the X-rays under these conditions was 10^7 .

3.5 Conclusions

A first single-UV-photon detection characterization of RPWELL-based detectors was presented. It was focused on gain and avalanche distribution evaluation. Two detector configurations were tested: single-stage CsI-RPWELL and dual-stage, CsI-THGEM + Cu-RPWELL. Both detectors demonstrated a discharge-free operation at high gain, showing a clear Polya distribution of single-photoelectron avalanches. This has the potential for a high detection efficiency of single photoelectrons.

This study is the first step towards a full characterization of RPWELL-based UV detectors. Along with measurements and simulations of photoelectron extraction and collection efficiencies, a systematic study should be performed to evaluate the effects of highly ionizing background and UV detection capability at high rate events.

The good stable performance of the dual-stage configuration at a gain of 10^5 under irradiation with both UV and soft X-rays is promising. Further systematic studies are foreseen.

4 General summary

Two studies have been presented: systematic long-term characterization of various RPWELL detectors and initial characterization of single- and dual-stage RPWELL based UV-detectors.

In the first study, new materials and new production techniques were investigated. The results placed the LRS glass as a good candidate for future applications.

An important consequence of this work is the establishment of a systematic and methodical framework for gas-avalanche detector investigations. For the first time reproducible long-term gain stabilization investigations of the RPWELL were carried out. They revealed some interesting phenomena related to charging up and charge evacuation processes of the detector. These processes will be the content of future systematic studies.

In the second study, single- and dual-stage RPWELL-based configurations were evaluated as UV-photon detectors. Both configurations exhibited high gain and a Polya single-electron avalanche distributions. The dual-stage configuration was found very promising; a stable operation at a gain of $\sim 10^6$ was recorded with UV; stable operation was demonstrated at the presence of soft X-ray photons at a gain of 10^5 . This implies that the double-stage RPWELL-based detector could become a good candidate for future applications such as photon imaging for particle identification with RICH detectors, scintillation-light imaging in radiography, medical imaging and rare-events searches with noble-liquid detectors. Further studies of this configuration are foreseen.

5 References

- [1] R. Chechik et al., *Thick GEM-like hole multipliers: properties and possible applications*, *Nucl. Instrum. Methods Phys. Res. A* **535** (2004) 303
- [2] R. Chechik, A. Breskin and C. Shalem; *Thick GEM-like multipliers - a simple solution for large area UV-RICH detectors*, *Nucl. Instrum. Methods Phys. Res. A* **553** (2005) 35-40.
- [3] A. Buzulutskov, *Advances in Cryogenic Avalanche Detectors*, *JINST* **7** (2012) C02025.
- [4] A. Bondar et al., *MPPC versus MRS APD in two-phase Cryogenic Avalanche Detectors*, *JINST* **10** (2015) P04013.
- [5] L. Arazi et al., *First results of a large-area cryogenic gaseous photomultiplier coupled to a dual-phase liquid xenon TPC*, *JINST* **10** (2015) P10020.
- [6] S. Duval et al., *On the operation of a micropattern gaseous UV-photomultiplier in liquid-Xenon*, *JINST* **6** (2011) P04007.
- [7] A. Breskin et al., *A novel liquid-Xenon detector concept for combined fast-neutrons and gamma imaging and spectroscopy*, *JINST* **7** (2012) C06008.
- [8] I. Israelashvili et al., *A comprehensive simulation study of a Liquid-Xe detector for contraband detection*, *JINST* **10** (2015) P03030.
- [9] S. Bressler et al., *Beam studies of novel THGEM-based potential sampling elements for Digital Hadron Calorimetry*, *JINST* **10** (2015) P03030.
- [10] R. Santonico and R. Cardarelli, *Development of resistive plate counters*, *Nucl. Instrum. Methods Phys. Res.* **187** (1981) 377-380.
- [11] K. Nagai, *Thin gap chambers in ATLAS*, *Nucl. Instrum. Methods Phys. Res. A* **384** (1996) 219-221.
- [12] RD51 collaboration, *Development of Micro-Pattern Gas Detectors Technologies*, CERN-LHCC-2008-011/LHCC-P-001, 2008.
- [13] T. Alexopoulos et al., *A spark-resistant bulk-micromegas chamber for high-rate applications*, *Nucl. Instrum. Methods Phys. Res. A* **110-118** (2011) 640.
- [14] L. Arazi et al., *Laboratory studies of THGEM-based WELL structures with resistive anode*, *JINST* **9** (2014) P04011.
- [15] G. Bencivenni et al., *The micro-Resistive WELL detector: a compact spark-protected single amplification-stage MPGD*, *JINST* **10** (2015) P02008.
- [16] A. Rubin et al., *First studies with the Resistive-Plate WELL gaseous multiplier*, *JINST* **8** (2013) P11004.

- [17] A. Rubin, *THGEM-detector investigations: electron-avalanche asymmetry and operation with resistive anodes* (Master's thesis, Weizmann Institute of Science, Rehovot, Israel) JINST (2013).
- [18] W. Shockley, *Currents to conductors induced by a moving point charge*, *J. Appl. Phys* **9** (1938) 635
- [19] S. Ramo, *Currents induced by electron motion*, *Proceedings of the I.R.E.*, September 1939, 584.
- [20] H. Raether, *Electron Avalanches and Breakdown in Gases*, Butterworths (1964).
- [21] R. Cardarelli et al., *Progress in resistive plate counters*, *Nucl. Instrum. Methods Phys. Res. A* **263** (1988) 20-25.
- [22] J. T. Bromley, *Investigation of the Operation of Resistive Plate Chambers*, Master's thesis, The University of Manchester (1994), retrieved from <http://inspirehep.net/record/1339734/files/> .
- [23] S. Bressler et al., *Recent advances with THGEM detectors*, *JINST* **8** (2013) C12012.
- [24] S. Bressler et al., *First in-beam studies of a Resistive-Plate WELL gaseous multiplier*, *JINST* **11** (2016) P01005.
- [25] L. Moleri et al., *The Resistive-Plate WELL with Argon mixtures-a robust gaseous radiation detector*, *Nucl. Instrum. Methods Phys. Res. A [In Press]* (2016) arXiv:1603.04820, 2016.
- [26] L. Moleri et al., *In-beam evaluation of a medium-size Resistive-Plate WELL gaseous particle detector*, *JINST* **11** (2016) P09013.
- [27] F. Sauli, *Principles of operation of multiwire proportional and drift chambers*, 1977 CERN-77-09.
- [28] C. Broyles, D. Thomas and S. Haynes, *The Measurement and Interpretation of the K Auger Intensities of Sn 113, Cs 137, and Au 198*, *Physical Review* **89** (1953) 715.
- [29] D. Mörmann et al., *Operation principles and properties of the multi-GEM gaseous photomultiplier with reflective photocathode*, *Nucl Instrum Methods Phys Res A* **530** (2004) 258–274.
- [30] J. Byrne, *Statistics of electron avalanches in the proportional counter*, *Nuclear Instruments and Methods* **74** (1969) 291-296.
- [31] W. Blum, W. Riegler and L. Rolandi, *Particle Detection with Drift Chambers*, Springer Berlin Heidelberg, 2008.
- [32] P. M. M. Correia et al., *How charging up affects THGEM detectors gain*, in *The 18th RD51 collaboration meeting*, Aveiro, 2016.
- [33] M. Alexeevet et al., *The gain in Thick GEM multipliers and its time-evolution*, *JINST* **10** (2015) P03026.
- [34] M. Altunbas et al., *Aging measurements with the Gas Electron Multiplier (GEM)*, *Nucl. Instrum.*

Methods Phys. Res. A **515** (2003) 249-254.

- [35] C. Adloff et al., *Environmental study of a Micromegas detector*, LAPP (2009) hal.archives-ouvertes.fr.
- [36] T. Behnke et al., *The International Linear Collider Technical Design Report - Volume 4: Detectors*, arXiv:1306.6329 (2013).
- [37] Y. Wang, "Update on Chinese low resistive glass," in RD51 Mini-Week, CERN, Meyrin, Switzerland, December, 2015. Retrieved from: https://indico.cern.ch/event/457639/contributions/1128055/attachments/1202254/1750281/Chinese_low_resistive_glass.pdf.
- [38] B. Azmoun et al., "A Study of Gain Stability and Charging Effects in GEM Foils, in 2006 IEEE Nuclear Science Symposium Conference Record **6** (2006) 3847-3851.
- [39] M. Alfonsi et al., *Simulation of the dielectric charging-up effect in a GEM detector*, *Nucl. Instrum. Methods Phys. Res. A* **671** (2012) 6-9.
- [40] P. M. M. Correia et al., *A dynamic method for charging-up calculations: the case of GEM*, *JINST* **9** (2014) P07025.
- [41] M. Cortesi et al., *THGEM operation in Ne and Ne/CH₄*, *JINST* **4** (2009) P08001.
- [42] M. Cortesi et al., *Studies of THGEM-based detector at low-pressure Hydrogen/Deuterium, for AT-TPC applications*, *JINST* **10** (2015) P09020.
- [43] A. Laso Garcia et al., *High-rate timing resistive plate chambers with ceramic electrodes*, *Nucl. Instrum. Methods Phys. Res. A* **818** (2016) 45-50.
- [44] M. Morales et al., *Conductivity and charge depletion aging of resistive electrodes for high rate RPCs*, *JINST* **8** (2013) P01022.
- [45] B. Rebel et al., *High voltage in noble liquids for high energy physics*, *JINST* **9** (2014) T08004, 2014.
- [46] A. Breskin et al., *CsI-THGEM gaseous photomultipliers for RICH and noble-liquid detectors*, *Nucl. Instrum. Methods Phys. Res. A* **639** (2011) 117-120.
- [47] L. Gallego Manzano et al., *XEMIS: A liquid xenon detector for medical imaging*, *Nucl. Instrum. Methods Phys. Res. A* **787** (2015) 89-93.
- [48] A. Breskin, "Liquid Hole-Multipliers: A potential concept for large single-phase noble-liquid TPCs of rare events," in *6th International Symposium on large TPCs for Low Energy Rare Event Detection*, Paris, France, 2012.
- [49] R. Chechik and A. Breskin, "Advances in gaseous photomultipliers," *Journal Nucl. Instrum. Methods Phys. Res. A*, vol. 595, no. 1, pp. 116-127, 2008.

- [50] ALICE Collaboration, *ALICE: Technical proposal for a Large Ion collider Experiment at the CERN LHC*, CERN / LHCC 95-71.
- [51] W. Anderson et al., *Design, construction, operation and performance of a Hadron Blind Detector for the PHENIX experiment*, *Nucl. Instrum. Methods Phys. Res. A* **646** (2011) 35-58.
- [52] M. Alexeev et al., *THGEM-based photon detectors for the upgrade of COMPASS RICH-1*, *Nucl. Instrum. Methods Phys. Res. A* **732** (2013) 732.
- [53] G. Charpak et al., *Micromegas, a multipurpose gaseous detector*, *Nucl. Instrum. Methods Phys. Res. A* **478** (2002) 26-36.
- [54] A. Breskin, *New trends in low-pressure gaseous detectors*, in *Detectors in Heavy-Ion Reactions*, Springer, Berlin Heidelberg (1982) 44-62.
- [55] A. László et al., *Single electron multiplication distribution in GEM avalanches*, *JINST* **11** (2016) P10017.
- [56] J. Derré et al., *Fast signals and single electron detection with a MICROMEAS photodetector*, *Nucl. Instrum. Methods Phys. Res. A* **449** (2000) 314-321.
- [57] T. Zerguerras et al., *Understanding avalanches in a Micromegas from single-electron response measurement*, *Nucl. Instrum. Methods Phys. Res. A* **772** (2015) 76-82.
- [58] J. Va'vra et al., *Study of CsI photocathodes: volume resistivity and ageing*, *Nucl. Instrum. Methods Phys. Res. A* **387** (1997) 154-162.